Land Use Change and Coronavirus Emergence Risk

Maria Cristina Rulli[1*], Paolo D'Odorico[2*], Nikolas Galli[1], and David T.S. Hayman[3]

[1] Department of Civil and Environmental Engineering, Politecnico di Milano, Piazza Leonardo da Vinci, 20133 Milano, Italy.

[2] Department of Environmental Science, Policy, and Management, University of California, Berkeley, California, USA.

[3] Molecular Epidemiology and Public Health Laboratory, School of Veterinary Science, Massey University, New Zealand.

* Maria Cristina Rulli **Email:** mariacristina.rulli@polimi.it

* Paolo D'Odorico **Email:** paolododo@berkeley.edu

Sentence summarizing manuscript

Wildlife reservoirs for SARS-coronavirus-2 live in global hotspots of forest fragmentation, livestock, and human density in China

Classification

APPLIED ECOLOGY

ENVIRONMENTAL STUDIES

Keywords

COVID19, Land Use Change, One Health, Livestock, Wildlife

This PDF file includes:

Main text
Figures 1 to 4
Supporting information (SI) Tables 1 to 3, Figure 1 to 8

Abstract

Coronavirus disease 2019 (COVID-19) and severe acute respiratory syndrome (SARS) causing coronaviruses are mostly discovered in Asian horseshoe bats. It is still unclear how ongoing land use changes may facilitate SARS-related coronavirus transmission to humans. Here we use a multivariate hotspot analysis of high-resolution land-use data to show that regions of China populated by horseshoe bats are hotspots of forest fragmentation, livestock and human density. We also identify areas susceptible to new hotspot emergence in response to moderate expansion of urbanization, livestock production, or forest disturbance, thereby highlighting regions vulnerable to SARS-CoV spillover under future land-use change. In China population growth and increasing meat consumption associated with urbanization and economic development have expanded the footprint of agriculture, leading to human encroachment in wildlife habitat and increased livestock density in areas adjacent to fragmented forests. The reduced distance between horseshoe-bats and humans elevates the risk for SARS-related coronavirus transmission to humans.

Introduction

The ongoing severe acute respiratory syndrome coronavirus-2 (SARS-CoV-2) pandemic is claiming human lives and disrupting the functioning of human societies in unprecedented ways. Where did this virus come from and how did it transmit to humans? What facilitated such a host shift and how can we prevent this from happening again? These are important questions, in addition to the most outstanding ones about whether, when, and how this pandemic will end.

Recent years have seen a rise in the recorded number of epidemics from emerging diseases. Such epidemics constitute a major public health threat because of our limited knowledge of prevention and treatment therapies. Most emerging infectious diseases originate from pathogen spillovers from wildlife to humans (1). Why are such outbreaks increasing? Does environmental change play a role?

Crucial to understanding the emergence of infectious diseases is the analysis of the factors facilitating the spillover from wildlife prior to further spread within human populations (2,3). In the case of SARS-CoV-2 genomic sequencing has shown that the virus is most closely related (~96%) to a strain present in horseshoe bats (4). It is still unclear whether the spillover of SARS-CoV-2 occurred directly from bats to humans or through an intermediate species. For instance, a strain of coronavirus very similar to SARS-CoV-2 was detected in Malayan Pangolin (*Manis javanica*) (5), a wild mammal that is frequently illegally smuggled from Southeast Asia into China and sold in markets (5). Regardless of the specific pathway, the pathogen flow of emerging zoonotic diseases to humans is the result of human interactions with wildlife. We argue that the increasing incidence of emerging disease outbreaks is the result of a similar set of drivers able to change the distance and contact rates between wildlife and humans (as well as human-human interaction), including population growth, urbanization, increasing affluence in mid-income countries, and the associated dietary shifts (6). As countries become more affluent demand for animal products increases, leading to an expansion of agriculture and animal husbandry, often at the expense of natural ecosystems (7). Human penetration in wildlife habitat favors the interaction between humans and wildlife species, either directly through activities like hunting or through other species, particularly livestock that are in closer contact with humans (8-11). The establishment of pastures, plantations or concentrated livestock farms close to forest margins may increase pathogen flows from wildlife to humans (2,9,11-14). Indeed, deforestation and

forest fragmentation themselves reshape the dynamics of wildlife communities, possibly leading to the extinction of habitat specialist species, while allowing generalists to thrive (15).

While several reports in the media have conjectured on a possible link between land use change and the emergence of the COVID19 pandemic, such a hypothesis still has to be supported by a comprehensive high-resolution analysis of land use patterns that combines forest fragmentation to livestock and human encroachment in wildlife habitat (2). Here we analyze environmental changes to explain why China remains at risk for other SARS-related coronavirus outbreaks (1,2). We analyze a set of factors that could make China a suitable location for the spillover to humans to occur. To that end, while we do not specifically link environmental change or bats as the immediate hosts of the SARS-CoV-2 ancestor (4,5), we use horseshoe bats in the genus *Rhinolophus* (family Rhinolophidae) as a model system to understand the risk of future coronavirus outbreaks because China is reported to be a region with both highly diverse horseshoe bats and bat SARS-like CoV (16-18).

Results

Among the four CoV genera, two (alpha- and betacoronaviruses) are found in bats. Among the betacoronaviruses, all four subgenera have been discovered in bats, including the SARS-related CoVs (SARSr-CoV, subgenera *Sarbecovirus*) (16-18). Both SARS-CoV-1 and Swine acute diarrhoea syndrome coronavirus (SADS-CoV) emerged in southeast China and were later detected in horseshoe bats, mainly *Rhinolophus sinicus* and *Rhinolophus affinis* (4,16-18). Most SARSr-CoVs are detected in horseshoe bats, although some strains have been detected in other genera. SARSr-CoVs in China are most similar to the highly pathogenic human SARS-CoVs (4,16-18). Therefore, we performed our local analyses of disturbance at bat locations to horseshoe bats in China (Fig 1a; Table S1) and our analyses of disturbance within horseshoe bat distributions in both the larger South, East, and South East Asia region and then China.

Within these distributions we generated 10000 random sampling points (Fig 1a, see SI). Within 30km from every random sampling point we calculate livestock density (n/km^2), forest cover and fragmentation, cropland cover, population density, and the fractional cover of human settlements (see Supplementary Materials) (14). Hotspots were calculated (Fig 1a) using the Getis-Ord algorithm to show the areas with high or low values of land use attributes cluster (Fig 2).

China exhibits a relatively high concentration of livestock production in horseshoe bat distributions (Fig 1a, Table S1). Indeed, China is a hotspot of livestock density within this region (Fig 1b), with statistically significant higher concentrations of chickens, ducks, pigs, goats and cattle (Fig 2a). Within a 30km radius from observed bat locations the density of chicken, ducks, pigs, goats, and cattle was again significantly greater than randomly selected locations. Conversely the sheep density is lower in China, though sheep density was low overall, as it was for other ruminants. The density of chickens, pigs, goats and cattle surrounding (<30km) the points where these bats were recorded and at the randomly selected locations in China within the suitability region were not significantly different, indicating that these random locations have livestock densities that are representative of the areas in which the actual presence of horseshoe bats has been documented.

Forest cover and fragmentation have been related to virus outbreaks from wildlife (including bats) for other zoonotic diseases such as Ebola virus disease (14). China exhibits on average lower forest cover and cropland density and greater forest fragmentation than the other regions analyzed (Fig

1c). The average forest cover and forest fragmentation in the surroundings (within 30km distance) of random points selected in China and the other regions (Figs 1a, 2b) show that these differences are statistically significant. Likewise, statistically significant differences (i.e. lower average cover and higher average fragmentation) are found between the points of actual observations of horseshoe bats and randomly selected locations in the regions outside China within the distributions of these bats (Fig 2b).

China also exhibits higher levels of human presence in horseshoe bat distributions, as evidenced by population density and the fraction of the landscape covered by villages, towns, and other human settlement (Fig 2c). Indeed, the region of China suitable for horseshoe bats coincides with hotspots of human settlements (Fig 1d). Collectively, these results demonstrate that China exhibits stronger signs of human encroachment, livestock density, and forest disturbance of SARSr-CoV hosting horseshoe bat distributions than other regions. In China, regions close to forest fragments are more densely used for livestock production and human settlements – and consequently exhibit lower forest and cropland cover (Fig 1b) – thereby favoring the contact between wildlife and humans either directly or through intermediate animals such as livestock. The fact that China is a global hotspot in the concurrence of these three factors (fragmentation, livestock density, and human settlement) is highlighted by the multivariate hotspot analysis (Fig. 3). These three attributes account for bat habitat (fragmentation), livestock, and human presence, which are major factors contributing to the spillover of zoonotic infectious diseases. Interestingly, we find that China is the global hotspot of simultaneously high forest fragmentation, livestock density and human settlement. The other major global hotspots outside China are found in Java, Bhutan, east Nepal, northern Bangladesh, the Kerala state of India and North-East India, the latter of which are known for past outbreaks of Nipah virus, another bat-related zoonotic disease (19).

We then use the multivariate hotspot framework to identify regions at high potential risk of SARSr-CoVs spillovers to humans as a result of land use change. To that end the results of the multivariate hotspot analysis were clustered in 30 groups, based on geographic contiguity and similarity in the above three attributes (Fig. 4a; Table S3). We then perturbed one attribute at a time in each group to evaluate that group's susceptibility to transitioning from non-significant conditions (Fig. 3) to a hotspot state (Fig. 4b). This sensitivity analysis (Fig 4b) shows areas at risk of transitioning to hotspots as a result of a future increase in at least one of the analyzed attributes (i.e. forest fragmentation, livestock density, or human settlement). Interestingly the Chinese region south of Shanghai is at high risk of potentially turning into a hotspot as a result of fragmentation increase. Other regions susceptible to hotspot transition as a result of forest fragmentation include Japan and north Philippines. Likewise, the transition region between China's hotspot and Indochina's coldspot and the region surrounding the hotspot of Thailand could turn into hotspots for SARSr-CoV spillover as a result of increasing presence of livestock or humans, respectively (Fig. 4b). These results point both to regions of the world currently suitable for SARSr-CoV spillover from wildlife to humans as well as those at risk of becoming prone to spillover as a result of trajectories of land use change and human penetration (Fig. 4c; Fig.S8 SI)

Discussion

Our approach uses the horseshoe bats as a model family because of their key role as hosts of *Sarbecovirus* coronaviruses, which have caused SARS, COVID-19, and SADS (4,13-18). Other

158 strains of related viruses have been found in other bat genera, but these relationships are less
159 clear (16-18). The widespread sampling of other bats may find species-specific relationships,
160 though horseshoe bats appear to be the reservoirs where most SARSr-CoVs have their
161 evolutionary ancestors so we assume they are the most appropriate model. The risk to humans
162 from other coronaviruses, therefore, will be different, because their host distributions are
163 different, and two CoV genera (gamma- and delta-coronaviruses) are mostly bird viruses.

164 The bat location data and species distribution data also suffer from different, but related issues.
165 The bat location data are presence only data. True absence data are difficult to obtain, therefore
166 we randomly sampled within different locations to generate pseudo-absence data. Choosing
167 where to sample from also present difficulties, so we chose horseshoe bat distribution data for
168 species that existed within China, East Asia, South, and South East Asia. This presents further
169 issues as the distribution of one species, the greater horseshoe bat (*Rhinolophus ferrumequinum*),
170 extends from Western Europe, Northern Africa, Central Asia and Eastern Asia. We therefore
171 weighted our sampling based on the number of overlapping species distributions to account for
172 this. However, these species distributions are large polygons and the realized niches used within
173 them by the species likely differ, so better niche models using presence and, ideally,
174 presence/absence data are required to develop better species presence predictions (20).
175 However, our results for random locations in China and outside China and reported bat
176 observations were comparable.

177 More generally, though using the relatively specific bat and virus relationships, we took a high-
178 level approach to understand the more distal or ultimate (rather than proximal) causes of
179 infectious disease emergence in China, linking environmental change and human drivers like
180 agricultural intensification. Different infectious diseases have different transmission mechanisms
181 and life cycles, and not all will respond to such changes in the same way. For example, directly
182 transmitted, acute infections with short incubation and infectious periods, like SARSr-CoVs, will
183 likely be dependent on hosts having greater densities, like in China, for them to emerge. The
184 epidemic potential is then also increased through local and global movement and trade, either of
185 people, wildlife, or livestock (8,21-23). Along with the biological properties of the virus and hosts,
186 the true risk of both the initial cross-species transmission and epidemic potential is either
187 increased or limited by more proximal mechanisms, such as biosecurity, health and safety
188 measures (e.g. personal protective equipment, meat hygiene) that can reduce risk, even if the
189 ultimate factors are present and increasing through the processes of habitat fragmentation and
190 human encroachment (8,14).

191 Spillover of infectious disease such as SARS, COVID-19 and SADS from wildlife to humans likely
192 requires the coexistence of horseshoe bats and humans in the same environment and is favored
193 by the presence of intermediate animal species, particularly livestock because it is in closer
194 contact with humans. The fragmentation and disturbance of forest ecosystems likely favors
195 habitat generalist bat species. In particular, chickens, ducks, and pigs have been associated with
196 the spread of several zoonotic viral infections, such as influenza viruses. This study demonstrates
197 that in China these important factors responsible for reducing the distance between wildlife and
198 humans co-occur both in horseshoe bat distributions and in the surroundings of actual
199 documented bat occurrence. These results are consistent with the notion that population growth
200 and increasing meat consumption associated with urbanization and economic growth have
201 expanded the footprint of agriculture, leading to human encroachment in wildlife habitat and
202 increased livestock density in areas adjacent to fragmented forest patches. China has dramatically

increased animal consumption (24), likely as the result of increasing affluence. In China, meat supply is largely reliant on domestic production using imported feed (e.g. soy from the Americas) (24), which explains the high livestock density in many rural areas, including those at the forest margins. Likewise, economic growth and the shift to diets richer in animal products explains the increasing demand for wild animal meat delicacies, increasing human-wildlife interactions through multiple pathways and the disturbance of forest habitat in more remote locations – frequently abroad – through trade-related teleconnections (25).

The multivariate hotspot analysis highlights how China is the largest hotspot for the concurrence of high forest fragmentation, livestock density, and human presence in our analysis (Fig. 3). The sensitivity analyses identifying the possible transition to new hotspots in response to an increase in one of these attributes (Fig. 4b) highlights areas that could become suitable for spillover and the type of land use change that could induce hotspot activation. Therefore, this analysis highlights region-specific targeted interventions that are urgently needed to increase resilience to SARSr-CoV spillovers. For instance, the green dots in Fig. 4 could be turned into hotspots as a result of forest fragmentation. In these regions resilience can be built through forest conservation or restoration efforts. Indeed, land use change evaluations should consider the risk of activating new hotspots suitable for wildlife-to-human spillover of pathogens such as SARSr-CoV, an aspect that has seldom been included in the impact analysis of land use change. Likewise, other regions such as the China-Indochina transition zone or central Thailand are prone to hotspot transitioning as a result of increased livestock density of urbanization, respectively. In these cases, mitigation of SARSr-CoV emergence can been enhanced by reducing livestock or human density, respectively, thereby inverting ongoing dietary and urbanization trends. Thus, environmental health, is tightly connected to both animal and human health, as recently stressed by planetary and 'one health' discourses, which advocate for more holistic views of global health, encompassing environment, animals, and people as well as their interactions (26).

Materials and Methods

Bat location data

Most SARS-related CoVs are detected in horseshoe bats, although some strains have also been detected in other genera (22,27-33). SARSr-CoVs in China are most similar to the highly pathogenic human SARS-CoVs (34-36).

We restricted our local analyses of disturbance at bat locations to Rhinolophid bats in China. We performed a Web of Science® search on 10/04/2020 using the following Boolean Operators: Rhinoloph* AND China AND Monitor* OR Survey OR Niche OR Distribution. We found 129 unique references. We removed all those published before 2000, reporting data outside China, review articles, and non-English (specifically 23 Chinese language publication), those with no Rhinolophid data, and those reporting only fossil records. We kept infection studies. This left 48 publications. We then further manually reviewed the publications for those reporting location data (22) but more specifically those with latitude and longitude, leaving 17 publications and 264 observations (see Fig. 1a; Table S1).

Bat distribution data

We restricted our analyses of disturbance in bat distributions to Rhinolophid bats in both the larger South, East and South East Asia region (but see main manuscript) and then China. We searched the IUCN Red List database (https://www.iucnredlist.org/search) using Taxonomy:

Rhinolophidae and Region: East Asia and South & South East Asia (herein 'regional') followed by Taxonomy: Rhinolophidae and Region: East Asia: China, Hong Kong & Taiwan (herein 'Chinese') classifications and downloaded the shapefiles for the 55 regional and 22 Chinese Rhinolophus species present in the region. We consider these areas as regions of suitable habitat for Rhinolophidae. The extent of this study area exceeds 28.5 million km^2.

Within these putative species distributions, we generated 10000 random sampling points with a local sampling density that is proportional to the number of species whose distributions were reported at the point. For every random sampling point we consider a circular area of 30km radius within which we calculate livestock density, forest cover and fragmentation, cropland cover, population density and the fractional cover of human settlements as explained below. The average values of these statistics are then calculated for China and the other regions of the world with habitat suitable for Rhinolophidae and compared and the difference is tested for significance using the Mann-Whitney non-parametric test in Mathematica©.

Livestock, forest cover, and population data

We took livestock data from the GeoWiki database that provides georeferenced livestock counts (in heads/km^2) at 1 km resolution for chickens, ducks, pigs, goats, sheep, and cattle (https://livestock.geo-wiki.org/home-2/). We quantified human presence both in terms of population density at 1 km resolution and as fraction of the landscape taken by villages, towns or other settlements from the WorldPop database at 1 km resolution. We used cropland data (at $30\times30m^2$ resolution) from (37). Forest cover data are available at 30m resolution annually between 2000 and 2018 (38). Forest cover is associated with the presence of trees taller than 5 m. Forest loss or gain was determined as the difference in forest cover between these two years.

Forest fragmentation analyses

We performed a forest fragmentation analyses based on Vogt et al. (39) using the 30m forest cover data. This method distinguishes forest cores, from forest margins and patches. Every 30m pixel is classified as wooded or non-wooded, based on whether its tree cover was greater or smaller than 50% in the year 2018. Forest cores are wooded pixels that are not adjacent to non-wooded pixels. Conversely, forest patches are made of wooded pixels that are not adjacent to forest core pixels. Wooded pixels that are neither core nor patch pixels occur at the margins of forest cores. Forest fragmentation was then quantified in terms of a composite fragmentation index (CFI) (13), defined as the ratio between the sum of number of pixels classified as "margins", "patches", or smaller core areas (i.e.,<200 ha), and the total number of pixels (wooded + non-wooded) in the 30km circles used to characterize land cover and land use in the surroundings of the points of actual bat observations or the randomly generated points. This index ranges between 0 and 1.

Hotspot Analyses and multivariate clustering

We mapped statistically significant hotspots of livestock density, forest fragmentation, and human settlements. To be a hotspot, an area needs to have a high (or low, in the case of cold-spots) value of its attribute and be also surrounded by other areas with high (or low) values of the same attribute. To that end, the 30km circles centered on the 10000 random points (Fig. 1a) considered in this study were used to carry out a hotspot analysis applying the Getis-Ord algorithm (Gi* statistics). The Gi* statistic shows to what extent areas with high or low values tend

to cluster thereby forming a hotspot. The result of the Gi* analysis is reported in terms of statistically significance with 90%, 95%, and 99% confidence (Fig. 1).

We then used two different methods to generate a multivariate distribution for the three indicators (livestock density, forest fragmentation and human settlements). First, we averaged their Gi*. Since the Gi* is a z-score, i.e. it has a standard normal distribution, a linear combination of the three Gi* indicators, such as their average, is a standard normal distribution and can still be represented with the same significance levels (Fig. 2). Second, we performed a spatially constrained multivariate clustering analysis. A Minimum Spanning Tree (MST) from the connectivity graph of the features was built, and then the SKATER (Spatial "K"luster Analysis by Tree Edge Removal) clustering method was used (40). The SKATER iteratively cuts branches in the MST, based on data variability among and within groups and on a spatial constraint, until it reaches the user-defined number of groups. The spatial constraint defined here is a k nearest neighbors type with 8 neighbors, meaning each feature in a group must have at least one of its 8 nearest neighbors in the same group. We chose 30 as the number of groups, calculated a set of summary statistics and boxplots for the groups and compared them to their global values (Table S2). For each indicator, we calculated the R^2 value as the reduction in variance of the indicator obtained by grouping, divided by the original variance of the indicator (Table S2). While the modularity analysis based on pseudo F-statistics shows that the optimal number of groups (the maximum differences between groups while maximizing within group similarity) is 12, here we studied 30 groups to analyse distinct regional patterns. Having a greater number of groups allows us to identify groups that are susceptible to transitioning to a hotspot because they are not "too different" from hotspots.

Acknowledgments

M.C.R and N.G. are supported by Cariplo Foundation (SusFeed project 0737 CUP D49H170000300007). D.T.H. is supported by USDA Hatch Multistate project no. W4190 capacity fund; Rutherford Discovery Fellowship RDF-MAU1701.

Competing interest statement: The authors declare no competing interests.

Author contributions: M.C.R. designed research; M.C.R. and D.T.S.H performed research; M.C.R., P.D. and N.G. analyzed data; P.D., M.C.R. and D.T.S.H wrote the paper.

References

1 K. E. Jones, N. G. Patel, M. A. Levy, A. Storeygard, D. Balk, J. L. Gittleman, P. Daszak, Global trends in emerging infectious diseases. *Nature* **451**, 990-993 (2008).

2 T. Allen, K. Murray, C. Zambrana-Torrelio, S. S. Morse, C. Rondinini, M. Di Marco, N. Brerit, K. J. Olival, P. Daszak, Global hotspots and correlates of emerging zoonotic diseases, *Nature Coomunications, **8**:* 1124, DOI: 10.1038/s41467-017-00923-8 (2017).

3 T. Wu C. Perrings, A. Kinzig, J. P. Collins, B. A. Minteer, P. Daszak, Economic growth, urbanization, globalization, and the risks of emerging infectious diseases in China: A review, *Ambio,* **46**:18–29.

4 Peng Zhou, Xing-Lou Yang, Xian-Guang Wang, Ben Hu, Lei Zhang, Wei Zhang, Hao-Rui Si, Yan Zhu, Bei Li, Chao-Lin Huang, Hui-Dong Chen, Jing Chen, Yun Luo, Hua Guo, Ren-Di Jiang, Mei-Qin Liu, Ying Chen, Xu-Rui Shen, Xi Wang, Xiao-Shuang Zheng, Kai Zhao, Quan-Jiao Chen, Fei Deng, Lin-Lin Liu, Bing Yan, Fa-Xian Zhan, Yan-Yi Wang, Geng-Fu Xiao & Zheng-Li Shi, A pneumonia outbreak associated with a new coronavirus of probable bat origin. *Nature* **579**, 270-273, (2020).

5 Tommy Tsan-Yuk Lam, Na Jia, Ya-Wei Zhang, Marcus Ho-Hin Shum, Jia-Fu Jiang, Hua-Chen Zhu, Yi-Gang Tong, Yong-Xia Shi, Xue-Bing Ni, Yun-Shi Liao, Wen-Juan Li, Bao-Gui Jiang, Wei Wei, Ting-Ting Yuan, Kui Zheng, Xiao-Ming Cui, Jie Li, Guang-Qian Pei, Xin Qiang, William Yiu-Man Cheung, Lian-Feng Li, Fang-Fang Sun, Si Qin, Ji-Cheng Huang, Gabriel M. Leung, Edward C. Holmes, Yan-Ling Hu, Yi Guan & Wu-Chun Cao, Identifying SARS-CoV-2 related coronaviruses in Malayan pangolins. *Nature*, (2020).

6 D. Tilman & M. Clark, Global diets link environmental sustainability and human health. *Nature* **515**, 518-522 (2014).

7 R. Naylor, Expanding the boundaries of agricultural development. *Food Security* **3**, 233 (2011).

8 D. A. Wilkinson, J. C. Marshall, N. P. French, D. T. Hayman, Habitat fragmentation, biodiversity loss and the risk of novel infectious disease emergence. *Journal of the Royal Society Interface* **15**, 20180403 (2018).

9 C. K. Johnson, P. L. Hitchens, P. S. Pandit, J. Rushmore, T. S. Evans, C. C. W. Young, M. M. Doyle, Global shifts in mammalian population trends reveal key predictors of virus spillover risk. *Proceedings of the Royal Society B* **287** (2020).

10 L. S. P. Bloomfield, T. L. McIntosh, E. F. Lambin, Habitat fragmentation, livelihood behaviors, and contact between people and nonhuman primates in Africa. *Landscape Ecology* **35**, 985-1000, doi:10.1007/s10980-020-00995-w (2020).

11 J. R. C. Pulliam, J. H. Epstein, J. Dushoff, S. A. Rahman, M. Bunning, A. A. Jamaluddin, A. D. Hyatt, H. E. Field, A. P. Dobson, P. Daszak, the Henipavirus Ecology Research Group (HERG), Agricultural intensification, priming for persistence and the emergence of Nipah virus: a lethal bat-borne zoonosis. *Journal of the Royal Society Interface* **9**, 89-101 (2012).

12 K. B. Chua , K. J. Goh, K. T. Wong, A. Kamarulzaman, P. S. Tan, T. G. Ksiazek, S. R. Zaki, G. Paul, S. K. Lam, C. T. Tan, Fatal encephalitis due to Nipah virus among pig-farmers in Malaysia. *The Lancet* **354**, 1257-1259 (1999).

13 Peng Zhou, Hang Fan, Tian Lan, Xing-Lou Yang, Wei-Feng Shi, Wei Zhang, Yan Zhu, Ya-Wei Zhang, Qing-Mei Xie, Shailendra Mani, Xiao-Shuang Zheng, Bei Li, Jin-Man Li, Hua Guo, Guang-Qian Pei, Xiao-Ping An, Jun-Wei Chen, Ling Zhou, Kai-Jie Mai, Zi-Xian Wu, Di Li, Danielle E. Anderson, Li-Biao Zhang, Shi-Yue Li, Zhi-Qiang Mi, Tong-Tong He, Feng Cong, Peng-Ju Guo, Ren Huang, Yun Luo, Xiang-Ling Liu, Jing Chen, Yong Huang, Qiang Sun,

Xiang-Li-Lan Zhang, Yuan-Yuan Wang, Shao-Zhen Xing, Yan-Shan Chen, Yuan Sun, Juan Li, Peter Daszak, Lin-Fa Wang, Zheng-Li Shi, Yi-Gang Tong, Jing-Yun, Fatal swine acute diarrhoea syndrome caused by an HKU2-related coronavirus of bat origin. *Nature* **5556**, 255-258(2018).

14 M. C. Rulli, M. Santini, D. T. Hayman, P. D'Odorico, The nexus between forest fragmentation in Africa and Ebola virus disease outbreaks. *Scientific reports* **7**, 41613 (2017).

15 C. F. Meyer, M. J. Struebig, M. R. Willig, in *Bats in the anthropocene: Conservation of bats in a changing world* 63-103 (Springer, Cham, 2016).

16 J. Cui, F. Li, Z. Shi, Origin and evolution of pathogenic coronaviruses. *Nature Reviews: Microbiology* **17**, 181-192(2019).

17 Y. Fan, K. Zhao, Z. Shi, P. Zhou, Bat coronaviruses in China. *Viruses* **11**, 1-11, (2019).

18 A. C. P. Wong, X. Li, S. K. P. Lau, P. C. Y. Woo, Global epidemiology of bat coronaviruses. *Viruses* **11**, doi:10.3390/v11020174 (2019).

19 V. Soman Pillai, G. Krishna, M. Valiya Veettil, Nipah Virus: Past Outbreaks and Future Containment. *Viruses.* **12**(4):465 (2020).

20 W. Thuiller, B. Lafourcade, R. Engler, M. B. Araújo, BIOMOD–a platform for ensemble forecasting of species distributions. *Ecography* **32**, 369-373 (2009).

21 M. Chinazzi, J. T. Davis, M. Ajelli, C. Giovannini, M. Litvinova, S. Merler, A. Pastore y Piontti, K. Mu, L. Rossi, K. Sun, C. Viboud, X. Xiong, H. Yu, M. E. Halloran, I. M. Longini Jr., A. Vespignani, The effect of travel restrictions on the spread of the 2019 novel coronavirus (COVID-19) outbreak. *Science* **368**, 395-400 (2020).

22 M. U. G. Kramer, C. Yang, B. Gutierrez, C. Wu, B. Klein, D. M. Pigott, Open COVID-19 Data Working Group, L. du Plessis, N. R. Faria, R. Li, W. P. Hanage, J. S. Brownstein, M. La, J. S. Brownstein, M. Layan, A. Vespignani, H. Tian, C. Dye, O. G. Pybus, S. V. Scarpino, The effect of human mobility and control measures on the COVID-19 epidemic in China. *Science* **368**, 493-497 (2020).

23 Q. Yang, X. Zhao, P. Lemey, M. A. Suchard, Y. Bi, W. Shi, D. Liu, W. Qi, G. Zhang, N. C. Stenseth, G. Pybus, H. Tian, Assessing the role of live poultry trade in community-structured transmission of avian influenza in China. *Proceedings of the National Academy of Sciences* **117**, 5949-5954 (2020).

24 P. D'Odorico, K. F. Davis, L. Rosa, J. A. Carr, D. Chiarelli, J. Dell'Angelo, J. Gephart, G. K. MacDonald, D. A. Seekell, S. Suweis, M. C. Rulli, The global food-energy-water nexus. *Reviews of Geophysics*, **56**, 456–531 (2018).

25 P. Meyfroidt, E. F. Lambin, K. H. Erb, T. W. Hertel, Globalization of land use: Distant drivers of land change and geographic displacement of land use. *Current Opinion in Environmental Sustainability*, **5**(5), 438–444 (2013).

26 S. Whitmee, A. Haines, C. Beyrer, F. Boltz, A. G. Capon, B. Ferreira de Souza Dias, A. Ezeh, H. Frumkin, P. Gong, P. Head, R. Horton, G. M. Mace, R. Marten, S. S Myers, S. Nishtar, S. A. Osofsky, S. K. Pattanayak, M. J. Pongsiri, C. Romanelli, A. Soucat, J. Vega, D. Yach, Safeguarding human health in the Anthropocene epoch: report of The Rockefeller Foundation–Lancet Commission on planetary health. *The Lancet* **386**, 1973-2028 (2015).

27 P. C. Y. Woo, S. K. P. Lau, C. S. F. Lam, C. C. Y. Lau, A. K. L. Tsang, J. H. N. Lau, R. Bai, J. L. L. Teng, C. C. C. Tsang, M. Wang, B. J. Zheng, K. H. Chan, K. Y. Yuen, Discovery of seven novel Mammalian and avian coronaviruses in the genus deltacoronavirus supports bat coronaviruses as the gene source of alphacoronavirus and betacoronavirus and avian

coronaviruses as the gene source of gammacoronavirus and deltacoronavirus. *J. Virol*., **86**, 3995–4008, (2012).

28 V. M. Corman, N. L. Ithete, L. R. Richards, M. C. Schoeman, W. Preiser, C. Drosten, J. F. Drexler, Rooting the Phylogenetic Tree of Middle East Respiratory Syndrome Coronavirus by Characterization of a Conspecific Virus from an African Bat. *J. Virol.,* **88**, 11297–11303, (2014).

29 ICTV 2018: Cornidovirineae. Available online: https://talk.ictvonline.org/taxonomy/p/taxonomy-history?taxnode_id=20186105 (2018).

30 C. Huang, W. J. Liu, W. Xu, T. Jin, Y. Zhao, J. Song, Y. Shi, W. Ji, H. Jia, Y. Zhou, H. Wen, H. Zhao, H. Liu, H. Li, Q. Wang, Y. Wu, L. Wang, D. Liu, G. Liu, H. Yu, E. C. Holmes, L. Lu, G. F. Gao, A Bat-Derived Putative Cross-Family Recombinant Coronavirus with a Reovirus Gene. *PLoS Pathog*, 12, e1005883 (2016).

31 P. C. Woo, M. Wang, S. K. Lau, H. Xu, R. W. Poon, R. Guo, B. H. Wong, K. Gao, H. W. Tsoi, Y. Huang, K. S. Li, C. S. Lam, K. H. Chan, B. J. Zheng, K. Y. Yuen, Comparative analysis of twelve genomes of three novel group 2c and group 2d coronaviruses reveals unique group and subgroup features. *J. Virol*., **81**, 1574–1585, (2007).

32 S. K. P. Lau, L. Zhang, H. K. H. Luk, L. Xiong, X. Peng, K. S. M. Li, X. He, P. S. Zhao, R. Y. Y. Fan, A. C. P. Wong, S.S. Ahmed, J.P. Cai, J. F. W. Chan, Y. Sun, D. Jin, H. Chen, T. C. K. Lau, R. K. H. Kok, W. Li, K. Y. Yuen, P. C. Y. Woo, Receptor Usage of a Novel Bat Lineage C Betacoronavirus Reveals Evolution of Middle East Respiratory Syndrome-Related Coronavirus Spike Proteins for Human Dipeptidyl Peptidase 4 Binding. *J. Infect. Dis*., **218,** 197–207 (2018).

33 S. K. Lau, P. C. Woo, K. S. Li, Y. Huang, H. W. Tsoi, B. H. Wong, S. S. Wong, S. Y. Leung, K. H. Chan, K. Y. Yuen, Severe acute respiratory syndrome coronavirus-like virus in Chinese horseshoe bats. *Proc. Natl. Acad. Sci. USA*, **102**, 14040–14045 (2005).

34 B. Hu, L. P. Zeng, X. L. Yang, X. Y. Ge, W. Zhang, B. Li, J. Z. Xie, X. R. Shen, Y. Z. Zhang, N. Wang, D. S. Luo, X. S. Zheng, M. N. Wang, P. Daszak, L. F. Wang, J. Cui, Z. L. Shi, Discovery of a rich gene pool of bat SARS-related coronaviruses provides new insights into the origin of SARS coronavirus. *PLoS Pathog*., **13**, e1006698 (2017).

35 K. G. Andersen, A. Rambaut, W. I. Lipkin, E. C. Holmes, R. F. Garry, The proximal origin of SARS-CoV-2. *Nature medicine*: **26**(4):450-452 (2020).

36 S. Lee, S. D. Jo, K. Son, I. An, J. Jeong, S. J. Wang, Y. Kim, W. Jheong, J. K. Oem, Genetic Characteristics of Coronaviruses from Korean Bats in 2016. *Microb. Ecol.,* **75**, 174–182, (2018).

37 P. Teluguntla, P. S. Thenkabail, J. Xiong, M. K. Gumma, C. Giri, C. Milesi, M. Ozdogan, R. Congalton, J. Tilton, T. R. Sankey, R. Massey, A. Phalke, K. Yadav, Global Cropland Area Database (GCAD) derived from Remote Sensing in Support of Food Security in the Twenty-first Century: Current Achievements and Future Possibilities. Chapter 7, Vol. II. Land Resources: Monitoring, Modelling, and Mapping, Remote Sensing Handbook edited by Prasad S. Thenkabail (2014).

38 M. C. Hansen, P. V. Potapov, R. Moore, M. Hancher, S. Turubanova, A. Tyukavina, D. Thau, S. V. Stehman, S. J. Goetz, T. R. Loveland, A. Kommareddy, A. V. Egorov, L. Chini, C. O. Justice, J. R. G. Townshend, High-resolution global maps of 21st-century forest cover change. *Science*, **342**:850–853 (2013).

458 39 P. Vogt, K. H. Riitters, C. Estreguil, J. Kozak, T. G. Wade, J. D. Wickham, Mapping spatial
459 patterns with morphological image processing. *Landscape Ecol*. **22**, 171–177 (2007).
460 40 R. M. Assuncao, M. C. Neves, G. Camara, C. Da Costa Freitas, Efficient Regionalisation
461 Techniques for Socio-economic Geographical Units using Minimum Spanning Trees.
462 *International Journal of Geographical Information Science* **20** (7): 797–811 (2006).

463
464
465

Figures main text

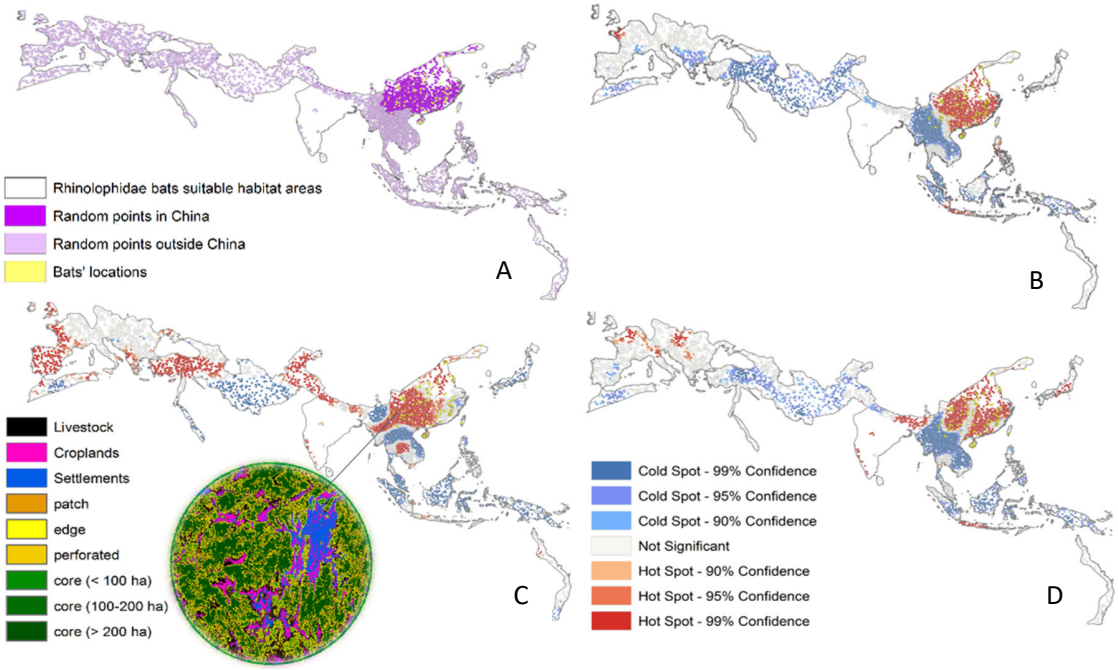

Figure 1. Univariate spatial analysis of coronavirus outbreak drivers (A) Sampling points randomly generated within China (dark purple) and outside China (light purple) and bat location points (yellow), weighted by the horseshoe bat species distributions present in East, South & South East Asia; (B) hotspots (red) and coldspots (blue) of livestock density; (C) hotspots of forest fragmentation; (D) hotspots of human settlement.

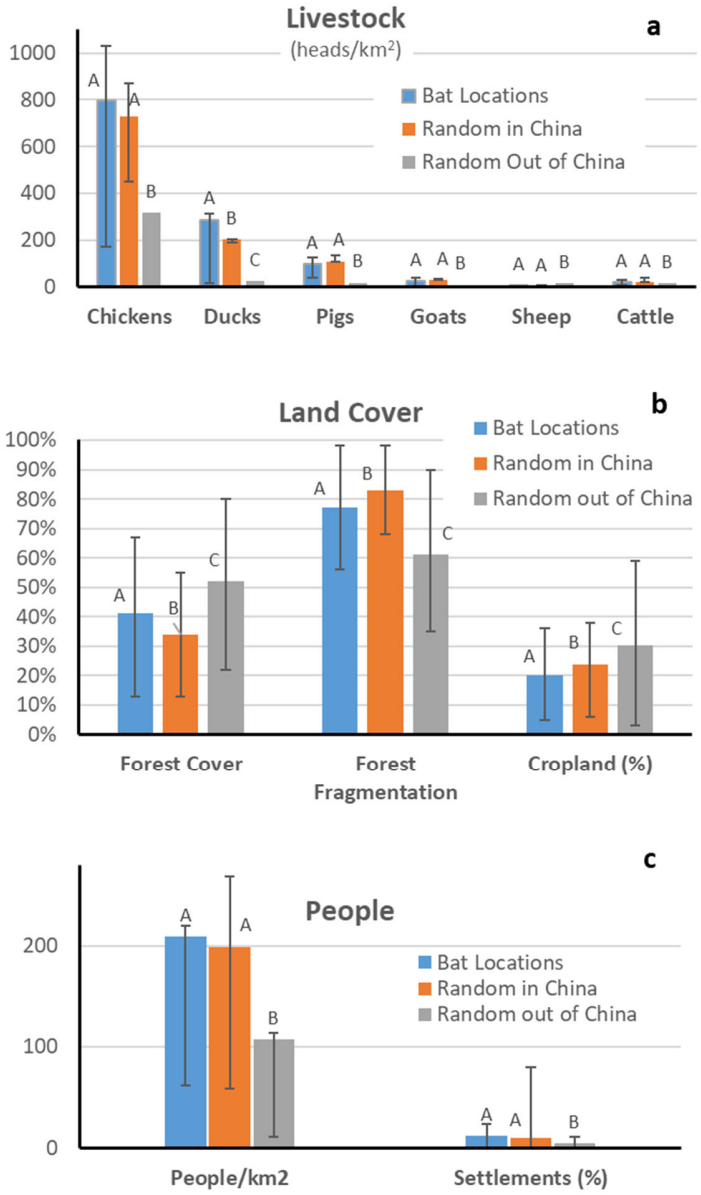

477

478

479 **Figure 2. Distribution comparison for coronavirus outbreak drivers.** Average distributions of
480 livestock (A), land cover and use (B), and human population (C) in areas likely suitable for
481 horseshoe bat occurrence in China and in the rest of their distribution. Error bars correspond to
482 the 20% and 80% percentiles. Different capital letters indicate statistically different means
483 (α=0.05).

484

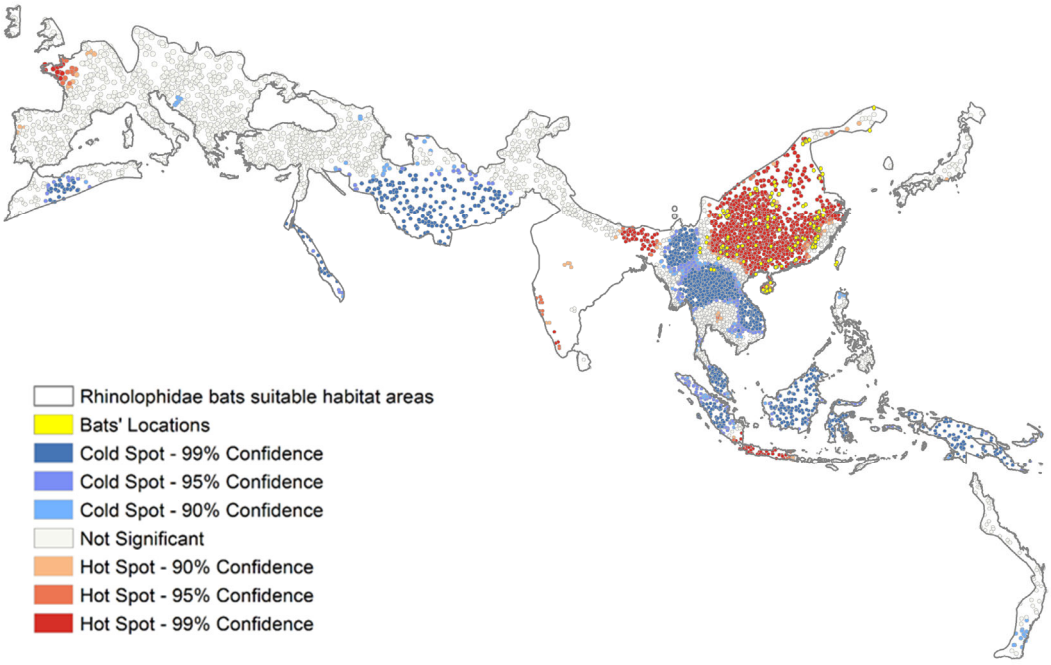

Figure 3. Multivariate spatial analysis of coronavirus outbreak drivers. Hotspot analysis based on the average Gi* Z-Score values for fragmentation, livestock density, and human settlements. Hotspots are classified based on their significance level.

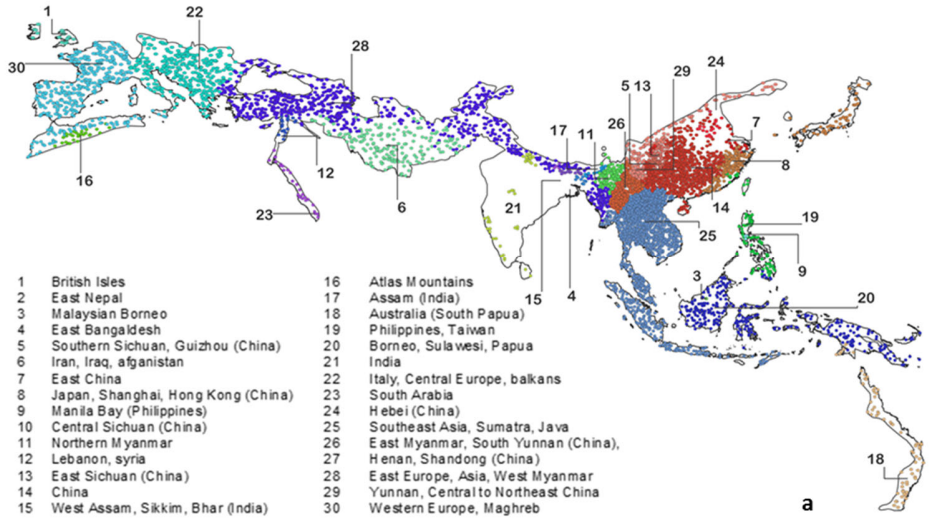

491

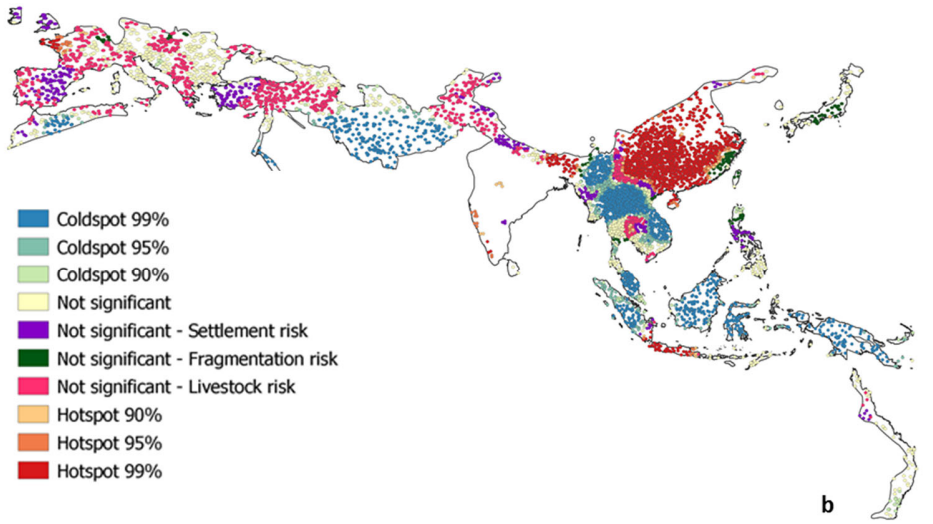

492

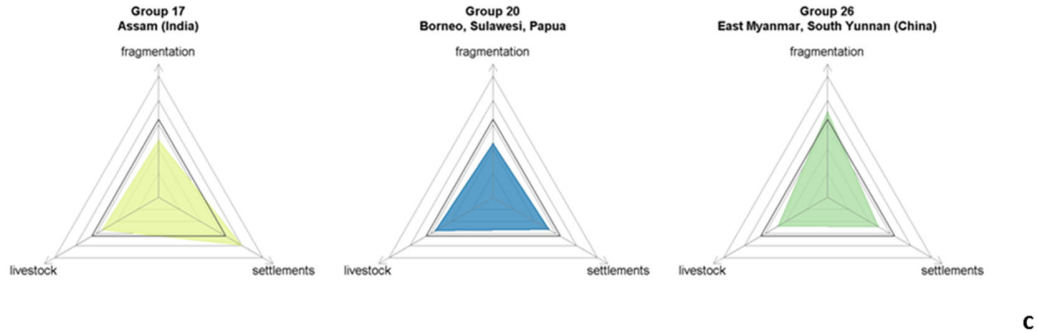

493

494 **Figure 4. Multivariate grouping analysis of coronavirus spillover drivers. (**A) Multivariate groups
495 analysis based on fragmentation, livestock and settlements attributes; (B) Areas at risk of

becoming hotspots as a result of changes in forest fragmentation (green), increase in livestock density (fuchsia) and human settlement (purple); (C) Possible trajectories of hotspot transition. These 3 groups represent areas not yet classified as hotspots (*not significant* by Gettis Ord analysis), but which may change trajectory. The solid triangle represents the safe space of variation for the 3 indicators (using multivariate Getis-Ord analysis).

Supplementary Materials

Environmental Change and Coronavirus Emergence Risk

Maria Cristina Rulli[1], Paolo D'Odorico[2], Nikolas Galli[1], David T.S. Hayman[3]

[1] Department of Civil and Environmental Engineering, Politecnico di Milano, Piazza Leonardo da Vinci, Milano, Italy

[2] Department of Environmental Science, Policy, and Management, University of California, Berkeley, California, USA

[3] Molecular Epidemiology and Public Health Laboratory, School of Veterinary Science, Massey University, New Zealand

Figures and Tables Supplementary Materials (SI)

Table S1. Horseshoe bat locations based on literature survey of studies reporting occurrences and related coordinates (coordinates are here listed as reported in the original articles and therefore they are not in a homogeneous format).

Species	Site	Location	Region	Latitude	Longitude	Ref.
R. macrotis	Shiyan Cave	Jing gang shan Nature Reserve	Jiangxi Province	26°36′N	114°12′E	[1]
R. macrotis	Xianren Cave	Jinning County	Yunnan Province	24°30′N	102°20′E	
R. macrotis	Tiantang Cave	Changtang County, Nanning city	Guangxi Province	22°49′N	108°42′E	
R. luctus	Emei shan	Emei shan	Sichuan province	29°31′11″N	103°19′57″E	[2]
R. formosae	Pingtung	Pingtung	Taiwan	22°40′16″N	120°29′17″E	
R. formosae	Kaohsiung	Kaohsiung	Taiwan	23°01′18″N	120°39′25″E	
R. affinis	Shiyan cave	Liping village, Jinggangshan Natural Reserve	Jiangxi Province	26°36′N	114°12′E	[3]
R. pearsoni	Shiyan cave	Liping village, Jinggangshan Natural Reserve	Jiangxi Province	26°36′N	114°12′E	
R. macrotis	Longxu cave	Shuanghe township	Yunnan Province	24°30′N	102°20′E	[4]
R. lepidus	Longxu cave	Shuanghe township	Yunnan Province	24°30′N	102°20′E	
R. sinisus	Longxu cave	Shuanghe township	Yunnan Province	24°30′N	102°20′E	
R. pusillus	Longxu cave	Shuanghe township	Yunnan Province	24°30′N	102°20′E	
R. ferrumequinum	Longxu cave	Shuanghe township	Yunnan Province	24°30′N	102°20′E	
R. rex	Longxu cave	Shuanghe township	Yunnan Province	24°30′N	102°20′E	
R. rex	Qianling Park	Guiyang	Guizhou province	26°36'58.0"N	106°41'26.6"E	[5]
R. ferrumequinum	Dalazi Cave	Zhi'an village, Ji'an city	Jilin Province	41°3′55.8″N	125°50′9.8″E	[6]
R. affinis		Jing Xi County Nature Preserve	Guangxi Autonomous Region	23◦07′12″ N	105◦57′36″ E	[7]
R. affinis		Shiwandashan National Nature Preserve	Guangxi Autonomous Region	21◦13′48″ N	107◦52′48″ E	
R. pearsonii		Dashahe Nature Preserve	Guizhou Province	29◦10′12″ N	107◦34′12″ E	
R. rouxii		Shiwandashan National Nature Preserve	Guangxi Autonomous Region	21◦13′48″ N	107◦52′48″ E	
R. rouxii	Shuipu	Maolan National Nature Preserve	Guizhou Province	25◦29′05″ N	107◦52′54″ E	
R. ferrumequinum		Huizhe	Yunnan	26:28:53	103:27:06	[8]
R. ferrumequinum		Baoxing	Sichuan	30:32:57	102:42:38	
R. ferrumequinum		Emei Shan	Sichuan	29:34:74	103:16:92	
R. ferrumequinum		Nanton	Sichuan	29:48:33	102:13:52	

R. ferrumequinum		Baiya	Shaanxi	33:21:32	108:03:36	
R. ferrumequinum		Foping	Shaanxi	33:34:00	107:59:00	
R. ferrumequinum		Shuangtai	Hubei	32:28:20	110:13:32	
R. ferrumequinum		Shuidong	Hubei	32:57:56	110:25:06	
R. ferrumequinum		Tiangou	Hubei	32:25:24	110:08:50	
R. ferrumequinum		Shenxian	Henan	34:41:49	113:22:05	
R. ferrumequinum		Shuanglongwan	Henan	33:58:28	110:56:57	
R. ferrumequinum		Yingyang	Henan	34:01:19	113:14:40	
R. ferrumequinum		Zhangjiashan	Henan	34:28:29	110:48:19	
R. ferrumequinum		Jindezhen	Jiangxi	29:19:44	117:11:48	
R. ferrumequinum		Wanfu	Jiangxi	28:05:47	117:01:46	
R. ferrumequinum		Jinzhai	Anhui	31:25:05	115:44:44	
R. ferrumequinum		Youkuang	Anhui	31:10:01	115:19:59	
R. ferrumequinum		Changshan	Shandong	34:59:37	117:58:44	
R. ferrumequinum		Nanzhi	Shandong	36:00:08	117:00:04	
R. ferrumequinum		Xiaya	Shandong	36:15:00	118:07:01	
R. ferrumequinum		Yinan	Shandong	35:31:06	118:24:40	
R. ferrumequinum		Beijing	Beijing	39:54:25	116:19:55	
R. ferrumequinum		Fangshan	Beijing	39:45:54	115:58:56	
R. ferrumequinum		Jietai	Beijing	39:54:35	116:14:55	
R. ferrumequinum		Jilin Shi	Jilin	43:46:49	126:29:56	
R. marshalli	Tiantang Cave	Tiantang village, Nanning city	Guangxi Province	4183955.80 N	12585099.80 E	[9]
R. ferrumequinum		Emei Shan	Sichuan	29°34′74″N	103°16′92″E	[10]
R. ferrumequinum		Foping	Shaanxi	33°34′00″N	107°59′00″E	
R. ferrumequinum		Daguping	Shaanxi	33°34′00″N	107°46′00″E	
R. ferrumequinum		Beijing	Hebei	39°54′25″N	116°19′55″E	
R. ferrumequinum	Fish cave		Anhui Province	30u209N	117u509E	[11]
R. sinicus		Qingyang, Anhui	Qingyang, Anhui	N30:20:511	E117:50:128	[12]
R. sinicus		Jingxian, Anhui	Jingxian, Anhui	N30:26:785	E118:24:783	
R. sinicus		Huashanmiku, Anhui	Huashanmiku, Anhui	N29:45:199	E118:23:331	
R. sinicus		Sanling mountain, Jiangxi	Sanling mountain, Jiangxi	N29:22:112	E117:34:324	
R. sinicus		Qingfeng cave, Jiangxi	Qingfeng cave, Jiangxi	N29:22:262	E117:39:357	
R. sinicus		Qinhui cave, Jiangxi	Qinhui cave, Jiangxi	N29:22:662	E117:32:335	
R. sinicus		Longhu mountain, Jiangxi	Longhu mountain, Jiangxi	N28:04:107	E116:58:227	
R. sinicus		Lijia country, Jiangxi	Lijia country, Jiangxi	N28:06:726	E116:59:282	
R. sinicus		Wuyishan baohuqu, Fujian	Wuyishan baohuqu, Fujian	N27:44:000	E117:40:000	
R. sinicus		Wuyishan tiliqiao, Fujian	Wuyishan tiliqiao, Fujian	N27:44:543	E117:29:953	
R. sinicus		Wuyishan Yanzijiao, Fujian	Wuyishan Yanzijiao, Fujian	N27:48:511	E117:42:505	
R. sinicus		Taihe, Jiangxi province	Taihe, Jiangxi province	N26:36:151	E114:12:734	
R. sinicus		Jinggang mountain, Jiangxi	Jinggang mountain, Jiangxi	N26:31:215	E115:06:610	
R. sinicus		Xingguo, Jiangxi	Xingguo, Jiangxi	N26:19:314	E115:35:229	
R. sinicus		Taining, Fujian	Taining, Fujian	N26:42:236	E117:29:867	
R. sinicus		Jiangle, Fujian	Jiangle, Fujian	N26:39:537	E117:34:387	
R. sinicus		Mingxi, Fujian	Mingxi, Fujian	N26:21:440	E117:11:398	
R. sinicus		Yongan, Fujian	Yongan, Fujian	N25:51:500	E117:17:000	
R. sinicus		Liancheng, Fujian	Liancheng, Fujian	N25:12:404	E117:15:066	
R. sinicus		Shanghang, Fujian	Shanghang, Fujian	N25:15:020	E116:49:009	
R. sinicus		Guilin, Guangxi	Guilin, Guangxi	N25:16:278	E110:17:009	
R. sinicus		Ruyuan, Guangdong	Ruyuan, Guangdong	N24:59:086	E113:08:523	
R. sinicus		Luofushan, Guangdong	Luofushan, Guangdong	N23:15:589	E114:03:656	
R. sinicus		Zhangjiajie, Hunan	Zhangjiajie, Hunan	N29:21:410	E110:34:783	
R. sinicus		Yongshun, Hunan	Yongshun, Hunan	N29:03:720	E109:38:358	
R. sinicus		Jishou, Hunan	Jishou, Hunan	N28:18:208	E109:39:175	
R. sinicus		Fenghuang, Hunan	Fenghuang, Hunan	N27:59:580	E109:33:786	

R. sinicus		Wuchuan, Guizhou	Wuchuan, Guizhou	N28:34:237	E107:54:058	
R. sinicus		Anlong, Guizhou	Anlong, Guizhou	N25:16:577	E105:31:931	
R. sinicus		Emeishan, Sichuan	Emeishan, Sichuan	N29:34:803	E103:24:708	
R. sinicus		Huize, Yunnan	Huize, Yunnan	N26:42:000	E103:30:000	
R. sinicus		Jiuxiang, Yunnan	Jiuxiang, Yunnan	N25:07:000	E103:22:000	
R. sinicus		Fumin, Yunnan	Fumin, Yunnan	N25:11:796	E102:27:863	
R. sinicus		Yongde, Yunnan	Yongde, Yunnan	N24:21:427	E099:02:161	
R. sinicus		Yinggeling, Hainan	Yinggeling, Hainan	N19:04:982	E109:33:107	
R. sinicus		Wuzhishan, Hainan	Wuzhishan, Hainan	N18:46:309	E109:31:012	
R. sinicus		Qiongzhong, Hainan	Qiongzhong, Hainan	N18:49:589	E110:00:435	
R. sinicus		Baoqing, Hainan	Baoqing, Hainan	N18:42:237	E109:41:528	
R. sinicus		Lingshui, Hainan	Lingshui, Hainan	N18:38:586	E109:57:636	
R. sinicus		Jianfengling, Hainan	Jianfengling, Hainan	N18:47:275	E108:57:364	
R. sinicus		Maogan, Hainan	Maogan, Hainan	N18:36:306	E109:26:776	
R. affinis	Shiyan cave	Liping village, Jinggangshan Natural Reserve	Jiangxi Province	26°360N	114°120E	[13]
R. pearsoni	Shiyan cave	Liping village, Jinggangshan Natural Reserve	Jiangxi Province	26°360N	114°120E	
R. macrotis		Yangchun	Guangdong Province	111.94	22.44	[14]
R. macrotis		Shaoguan	Guangdong Province	113.56	24.77	
R. macrotis		Nanning	Guangxi Province	108.70	22.82	
R. macrotis		Lengshuijiang	Hunan Province	111.57	27.75	
R. macrotis		Jianggangshan	Jiangxi Province	114.20	26.60	
R. macrotis		Jinning	Jinning	102.33	24.50	
R. macrotis		Yuanjiang	Yunnan Province	102.00	23.59	
R. macrotis		Baoshan	Yunnan Province	99.10	25.08	
R. macrotis		Wulong	Chongqing City	107.95	29.27	
R. macrotis		Yangchun	Guangdong Province	111.94	22.44	
R. macrotis		Xishui	Guizhou Province	106.21	28.45	
R. macrotis		Dazhou	Sichuan Province	107.74	31.20	
R. macrotis		Hanzhong	Shannxi Province	107.03	32.84	
R. macrotis		Xichuan	Henan Province	111.55	32.87	
R. macrotis		Wulong	Chongqing City	107.95	29.27	
R. macrotis		Lengshuijiang	Hunan Province	111.57	27.75	
R. macrotis		Jianggangshan	Jiangxi Province	114.20	26.60	
R. macrotis		Ganzhou	Jiangxi Province	114.09	25.46	
R. macrotis		Hanzhong	Shannxi Province	107.03	32.84	
R. sinicus		10km Mojiang, Zhenyuan, and Ning'er towns, Mojiang	Yunnan Province			[15]
R. affinis		10km Mojiang, Zhenyuan, and Ning'er towns, Mojiang	Yunnan Province			
R. schnitzleri	Xiao-dong Cave	Gengjiaying Commune, Yi-liang County, Kunming City	Yunnan province	25°02'N	103°14'E	[16]
R. affinis	Longkong Cave	Yanshi County	Fujian	25°12'N	117°15'E	[17]
R. affinis	Zhuxi Cave	Shanghang County	Fujian	25°10'N	116°45'E	
R. affinis	Jinkuang Cave	Liancheng County	Fujian	25°39'N	116°53'E	
R. affinis	Qixian Cave	Sha County	Fujian	26°25'N	117°39'E	
R. affinis	Guixian Cave	Mingxi County	Fujian	26°24'N	117°11'E	
R. affinis	Huanghuacong Cave	Yanzijiao Town, Wuyi Mountain	Fujian	27°49'N	117°43'E	
R. affinis	Shui Cave	Longmen County	Guangdong			
R. affinis	Dongbian Cave	Longmen County	Guangdong			
R. affinis	Penglai Cave	Yunfu Mount, Bolo County	Guangdong			
R. affinis	Fangkong	Luofu Mountain, Huizhou City	Guangdong	23°16'N	114°04'E	
R. affinis	Seven Star Cave	Guilin City	Guangxi	25°17'N	110°18'E	

R. affinis	Fenkeng Cave	Guilin City	Guangxi	25°17′N	110°21′E	
R. affinis	Seven Star Cave	Guilin City	Guangxi	25°17′N	110°18′E	
R. affinis	Bianfu Cave	Lingshui County	Hainan	18°42′N	109°53′E	
R. affinis	Xiashui Cave	Qiongzhong County	Hainan	19°04′N		
R. affinis	Qianlong Cave	Baoting County	Hainan	18°34′N	109°26′E	
R. affinis	Fangkong Cave	Yingge Mountain	Hainan	19°04′N	109°33′E	
R. affinis	Qishier Cave	Huoshan Mountain, Haikou City	Hainan	19°57′N	110°12′E	
R. affinis	Bianfu Cave	Xixia countryside	Henan			
R. affinis	Longhushan Park	Yingtan City	Jiangxi	28°04′N	116°58′E	
R. affinis	Jinuo Town	Xishuang banna	Yunnan	21°58′N	100°49′E	
R. affinis		Manfa Village, Xishuang banna	Yunnan			
R. affinis	Dashu Cave	Xishuangbanna	Yunnan			
R. affinis	Jiuxiang Cave	Yiliang County	Yunnan			
R. affinis	Shaft Cave, near Bailong Cave	Mile County	Yunnan	24°11′N	103°21′E	
R. ferrumequinum	Bianfu Cave	SW of Beijing	Beijing	39°43′N	115°43′E	
R. ferrumequinum	Shidu Caves	Fangshan District	Beijing	39°25′N	115°17′E	
R. ferrumequinum	Bianfu Cave	SW of Beijing	Beijing	39°43′N	115°43′E	
R. ferrumequinum	Bianfu Cave, Beijing	Bianfu Cave, Beijing	Beijing			
R. ferrumequinum	Guanyin Cave, Jietai Temple	Fang shan Town	Beijing	39°48′N	115°48′E	
R. ferrumequinum	Seven Star Cave	Guilin City	Guangxi	25°17′N	110°18′E	
R. ferrumequinum	Shenxian Cave	Huancuigu, Rongyang County	Henan	34°38′N	113°15′E	
R. ferrumequinum		Shennongjia	Henan	31°30′N	110°23′E	
R. ferrumequinum	Sihe Village	Langhe Town, Wudang Mountain	Henan			
R. ferrumequinum	Tong mu Village	Muyu Town, Tanjiawan County	Henan	31°28′N	110°25′E	
R. ferrumequinum	Wanfu Cave	Jing dezhen County	Jiangxi	28°37′N	116°28′E	
R. ferrumequinum	Juda Lizi Cave	Zian Village, Jian City	Jilin	41°04′N	125°50′E	
R. ferrumequinum	Xiaya Cave	Yiyuan County	Shandong			
R. ferrumequinum		Nantou Village, Luding County	Sichuan	29°48′N	102°14′E	
R. ferrumequinum	Dahu Cave	Emeishan	Sichuan	29°35′N	103°17′E	
R. ferrumequinum	Du Cave	Panshan Mountain, Tianjin City	Tianjin	25°33′N	116°60′E	
R. ferrumequinum	Heshang Cave	Kunming, Fumin County	Yunnan	25°12′N	102°28′E	
R. ferrumequinum	Xiaogou Cave	Kunming City	Yunnan	25°04′N	103°23′E	
R. ferrumequinum	Xiao Cave	Yiliang County	Yunnan			
R. lepidus	Tianlong Cave	Dali County	Yunnan	25°55′N	100°05′E	
R. lepidus	Xiyou Cave	Fumin County	Yunnan	25°09′N	102°39′E	
R. osgoodi	Tianlong Cave	Dali County	Yunnan	25°55′N	100°05′E	
R. osgoodi	Xiyou Cave	Fumin County	Yunnan	25°09′N	102°39′E	
R. luctus	Jiuba Cave	Jiangle County	Fujian	26°43′N	117°29′E	

R. luctus	Kangtou Cave		Fujian	26°40′N	117°36′E	
R. luctus	Xianren Cave	Shishan Town, Haikou City	Hainan	19°44′N	109°37′E,	
R. luctus	Tangle Cave	Jishou	Hunan	28°18′N	109°39′E	
R. macrotis	Shidu Caves	Beijing	Beijing			
R. macrotis	Closed Cave	Ziyuan County	Guangxi			
R. macrotis	Yuanfeng Cave	Qilai County	Sichuan	30°29′N	103°24′E	
R. siamensis	Yinhua Cave	Jiangle County	Fujian	26°39′N	117°34′E	
R. siamensis	Zhuxi Cave	Shanghang County	Fujian	25°10′N	116°45′E	
R. siamensis	Ganru Cave	Liancheng County	Fujian			
R. siamensis	Yinhua Cave	Jiangle County	Fujian	26°39′N	117°34′E	
R. siamensis	Seven Star Cave	Guilin City	Guangxi	25°17′N	110°18′E	
R. siamensis	Closed Cave	Ziyuan County	Guangxi			
R. siamensis	Wolong Cave	Xingyi County	Guizhou	24°9′N	104°53′E	
R. siamensis	Shanjia Cave	Anlong County	Guizhou	25°19′N	105°05′E	
R. siamensis	Wanfu Cave	Jing dezhen County	Jiangxi	28°37′N	116°28′E	
R. siamensis		Manfa Village, Xishuang banna	Yunnan			
R. siamensis	Heshang Cave	Kunming, Fumin County	Yunnan	25°12′N	102°28′E	
R. marshalli	Baisha Cave	Guiping County	Guangxi	23°14′N	109°54′E	
R. marshalli	Shepo Cave	Guiping County	Guangxi	23°25′N	110°15′E	
R. marshalli	Bailong Cave	Mile County	Yunnan	24°12′N	103°14′E	
R. marshalli	Gulong Cave	Yuanjiang County	Yunnan	23°35′N	101°58′E	
R. pearsonii	Yulong Cave	Qingyang County	Anhui	30°21′N	117°50′E	
R. pearsonii	Longkong Cave	Yanshi County	Fujian	25°12′N	117°15′E	
R. pearsonii	Yuhua Cave	Jiangle County	Fujian	26°39′N	117°35′E	
R. pearsonii	Bianfu Cave	Taining City	Fujian	26°42′N	117°30′E	
R. pearsonii	Ganru Cave	Liancheng County	Fujian			
R. pearsonii	Guwang Cave	Wuyi City	Fujian	27°42′N	117°42′E	
R. pearsonii	Huanghuacong Cave	Yanzijiao Town, Wuyi Mountain	Fujian	27°49′N	117°43′E	
R. pearsonii	Shang Cave	Dafu Village, Meihua Town, Lechang County	Guangdong	25°09′N	113°04′E	
R. pearsonii	Seven Star Cave	Guilin City	Guangxi	25°17′N	110°18′E	
R. pearsonii	Closed Cave	Ziyuan County	Guangxi			
R. pearsonii		Liangjiang Town, Wuming County	Guangxi			
R. pearsonii	Xipo Cave	Wuchuan County	Guizhou			
R. pearsonii	Wanfu Cave	Jing dezhen County	Jiangxi	28°37′N	116°28′E	
R. pearsonii	Bao Zi Cave	Tian Quan County	Sichuan	30°10′N	102°52′E	
R. pearsonii	Fufeng Cave	Emeishan	Sichuan	29°34′N	103°25′E	
R. pearsonii	Jiulao Cave	Emeishan	Sichuan	29°33′N	109°47′E	
R. pearsonii	Mingjiu Cave	Mongzi County	Yunnan			
R. pearsonii	Pingbian Village	Mongzi County	Yunnan			
R. pearsonii	Wangzhangya Cave	Dawei County	Yunnan			

R. pearsonii	Bianfu Cave	Mengla County	Yunnan	21°53′N	101°18′E	
R. yunanensis	Yulong Cave	Qingyang County	Anhui	30°21′N	117°50′E	
R. yunanensis	Longkong Cave	Yanshi County	Fujian	25°12′N	117°15′E	
R. yunanensis	Yuhua Cave	Jiangle County	Fujian	26°39′N	117°35′E	
R. yunanensis	Bianfu Cave	Taining City	Fujian	26°42′N	117°30′E	
R. yunanensis	Ganru Cave	Liancheng County	Fujian			
R. yunanensis	Guwang Cave	Wuyi City	Fujian	27°42′N	117°42′E	
R. yunanensis	Huanghuacong Cave	Yanzijiao Town, Wuyi Mountain	Fujian	27°49′N	117°43′E	
R. yunanensis	Shang Cave	Dafu Village, Meihua Town, Lechang County	Guangdong	25°09′N	113°04′E	
R. yunanensis	Seven Star Cave	Guilin City	Guangxi	25°17′N	110°18′E	
R. yunanensis	Closed Cave	Ziyuan County	Guangxi			
R. yunanensis		Liangjiang Town, Wuming County	Guangxi			
R. yunanensis	Xipo Cave	Wuchuan County	Guizhou			
R. yunanensis	Wanfu Cave	Jing dezhen County	Jiangxi	28°37′N	116°28′E	
R. yunanensis	Bao Zi Cave	Tian Quan County	Sichuan	30°10′N	102°52′E	
R. yunanensis	Fufeng Cave	Emeishan	Sichuan	29°34′N	103°25′E	
R. yunanensis	Jiulao Cave	Emeishan	Sichuan	29°33′N	109°47′E	
R. yunanensis	Mingjiu Cave	Mongzi County	Yunnan			
R. yunanensis	Pingbian Village	Mongzi County	Yunnan			
R. yunanensis	Wangzhangya Cave	Dawei County	Yunnan			
R. yunanensis	Bianfu Cave	Mengla County	Yunnan	21°53′N	101°18′E	
R. rex	Dongmen Cave	Fushui County	Guangxi			
R. rex	White Dragon Cave	Guilin City	Guangxi			
R. rex	Fenkeng Cave	Guilin City	Guangxi	25°17′N	110°21′E	
R. rex	Fenkeng Cave	Guilin City	Guangxi	25°17′N	110°21′E	
R. rex	Xipo Cave	Wuchuan County	Guizhou			
R. rex	Qingxuan Cave		Yunnan	26°40′N	100°12′E	
R. rex	Tianlong Cave	Dali County	Yunnan	25°55′N	100°05′E	
R. rex	Bianfu Cave	Yiliang County	Yunnan	25°04′N	103°23′E	
R. rex	Xiyou Cave	Fumin County	Yunnan	25°09′N	102°39′E	
R. rex	Xiaogou Cave	Yiliang County	Yunnan			
R. paradoxolophus	Dongmen Cave	Fushui County	Guangxi			
R. paradoxolophus	White Dragon Cave	Guilin City	Guangxi			
R. paradoxolophus	Fenkeng Cave	Guilin City	Guangxi	25°17′N	110°21′E	
R. paradoxolophus	Fenkeng Cave	Guilin City	Guangxi	25°17′N	110°21′E	
R. paradoxolophus	Xipo Cave	Wuchuan County	Guizhou			
R. paradoxolophus	Qingxuan Cave		Yunnan	26°40′N	100°12′E	
R. paradoxolophus	Tianlong Cave	Dali County	Yunnan	25°55′N	100°05′E	
R. paradoxolophus	Bianfu Cave	Yiliang County	Yunnan	25°04′N	103°23′E	
R. paradoxolophus	Xiyou Cave	Fumin County	Yunnan	25°09′N	102°39′E	

R. paradoxolophus	Xiaogou Cave	Yiliang County	Yunnan			
R. sinicus	Yinhua Cave	Jiangle County	Fujian	26°39′N	117°34′E	
R. sinicus	Bianfu Cave	Taining City	Fujian	26°42′N	117°30′E	
R. sinicus	Longkong Cave	Yanshi County	Fujian	25°12′N	117°15′E	
R. sinicus	Mine	Buyun Town, Shanghang County	Fujian	25°15′N	116°50′E	
R. sinicus	Jinkuang Cave	Liancheng County	Fujian	25°39′N	116°53′E	
R. sinicus	Liuhuang Cave	Liancheng County	Fujian	25°52′N	117°17′E	
R. sinicus	Yuxi Cave	Mingxi County	Fujian	26°21′N	117°11′E	
R. sinicus	Yinhua Cave	Jiangle County	Fujian	26°39′N	117°34′E	
R. sinicus	Xing Cave	Qiliqiao Bridge, Wuyi Mountain	Fujian	27°45′N	117°30′E	
R. sinicus	Mine, Chang ganzhou Road	Xincun Town, Wuyi City	Fujian	27°37′N	117°50′E	
R. sinicus	Huanghuacong Cave	Yanzijiao Town, Wuyi Mountain	Fujian	27°49′N	117°43′E	
R. sinicus	Penglai Cave	Yunfu Mount, Bolo County	Guangdong			
R. sinicus	Fangkong	Luofu Mountain, Huizhou City	Guangdong	23°16′N	114°04′E	
R. sinicus	Ni Cave	Xinyi County	Guangdong	22°20′N	110°57′E	
R. sinicus	Shuili Cave	Xinyi County	Guangdong	22°20′N	110°58′E	
R. sinicus	Kiln	Xinyi County	Guangdong	22°15′N	110°60′E	
R. sinicus	Closed Cave	Ziyuan County	Guangxi			
R. sinicus	Fenkeng Cave	Guilin City	Guangxi	25°17′N	110°21′E	
R. sinicus	Fenkeng Cave	Guilin City	Guangxi	25°17′N	110°21′E	
R. sinicus	Shui Cave	Guilin City	Guangxi			
R. sinicus	Jiang Cave	Jiangkou County	Guizhou	23°25′N	110°15′E	
R. sinicus	Xiashui Cave	Qiongzhong County	Hainan	19°04′N		
R. sinicus	Hela Village	Hongmao Town, Qiongzhong County	Hainan			
R. sinicus	Diyi Village	Five Finger Mountain	Hainan			
R. sinicus	Fangkong Cave	Jianfeng Mountain	Hainan	18°54′N	109°42′E	
R. sinicus	Cave	Yichang City	Hubei			
R. sinicus	Longhushan Park	Yingtan City	Jiangxi	28°04′N	116°58′E	
R. sinicus	Wanfu Cave	Jing dezhen County	Jiangxi	28°37′N	116°28′E	
R. sinicus	Fufeng Cave	Emeishan	Sichuan	29°34′N	103°25′E	
R. sinicus	Jiulao Cave	Emeishan	Sichuan	29°33′N	109°47′E	
R. sinicus	Bailong Cave	Mile County	Yunnan	24°12′N	103°14′E	
R. pusillus	Shidu Caves	Fangshan District	Beijing	39°25′N	115°17′E	
R. pusillus	Sanqing Cave	Wanglaopu, Fangshan District	Beijing	39°45′N	115°45′E	
R. pusillus	Longkong Cave	Yanshi County	Fujian	25°12′N	117°15′E	
R. pusillus	Yinhua Cave	Jiangle County	Fujian	26°39′N	117°34′E	
R. pusillus	Jinkuang Cave	Liancheng County	Fujian	25°39′N	116°53′E	
R. pusillus	Ganru Cave	Liancheng County	Fujian			

R. pusillus	Niutongguan Cave	Liancheng County	Fujian	25°33′N	116°59′E	
R. pusillus	Chuqi Cave	Liancheng County	Fujian	25°33′N	116°60′E	
R. pusillus	Liuhuang Cave	Liancheng County	Fujian	25°52′N	117°17′E	
R. pusillus	Qixian Cave	Sha County	Fujian	26°25′N	117°39′E	
R. pusillus	Yinhua Cave	Jiangle County	Fujian	26°39′N	117°34′E	
R. pusillus	Jiuba Cave	Jiangle County	Fujian	26°43′N	117°29′E	
R. pusillus	Cave of the Buddha	Dingushan Forest Eco system,	Guangdong			
R. pusillus	Butterfly Cave	Yunfu Mount	Guangdong			
R. pusillus	Fangkong	Luofu Mountain, Huizhou City	Guangdong	23°16′N	114°04′E	
R. pusillus	Dianxian Cave	Xinyi County	Guangdong	22°20′N	110°57′E	
R. pusillus	Shuili Cave	Xinyi County	Guangdong	22°20′N	110°58′E	
R. pusillus	Rock crevice	Xinyi County	Guangdong	22°15′N	111°00′E	
R. pusillus	Tongtian Cave	Xinyi County	Guangdong	22°23′N	110°72′E	
R. pusillus	Chang Cave	Xinyi County	Guangdong	22°17′N	111°02′E	
R. pusillus	Jishui Cave	Guilin City	Guangxi	25°17′N	110°21′E	
R. pusillus	White Dragon Cave	Guilin City	Guangxi			
R. pusillus	Seven Star Cave	Guilin City	Guangxi	25°17′N	110°18′E	
R. pusillus	Closed Cave	Ziyuan County	Guangxi			
R. pusillus		Liangjiang Town, Wuming County	Guangxi			
R. pusillus	Shui Cave	Guilin City	Guangxi			
R. pusillus	Shui Cave	Guilin City	Guangxi			
R. pusillus	Jishui Cave	Guilin City	Guangxi	25°17′N	110°21′E	
R. pusillus	Seven Star Cave	Guilin City	Guangxi	25°17′N	110°18′E	
R. pusillus	Wulong Cave	Mashan County	Guangxi			
R. pusillus	Shanjia Cave	Anlong County	Guizhou	25°19′N	105°05′E	
R. pusillus		Leigong Mountain	Guizhou			
R. pusillus	Fangkong Cave	Jianfeng Mountain	Hainan	18°54′N	109°42′E	
R. pusillus		Yichang City	Hubei	31°09′N	111°08′E	
R. pusillus	Shenlong Cave	Yichang	Hubei	31°21′N	110°30′E	
R. pusillus	Yeren Cave	Shennon gjia	Hubei	31°55′N	110°44′E	
R. pusillus	Sihe Village	Langhe Town, Wudang Mountain	Henan			
R. pusillus	Xianren Cave	Wuhan City	Hubei	25°53′N	114°30′E	
R. pusillus	Longhushan Park	Yingtan City	Jiangxi	28°04′N	116°58′E	
R. pusillus	Wanfu Cave	Jing dezhen County	Jiangxi	28°37′N	116°28′E	
R. pusillus	Xiaya Cave	Yiyuan County	Shandong			
R. pusillus	Mine	Buyun Town, Shanghang County	Shandong	25°15′N	116°50′E	
R. pusillus		Yilai Mountain	Sichuan	30°29′N	103°24′E	
R. pusillus		Luding County	Sichuan	29°48′N	102°14′E	
R. pusillus	Qilai County	Qilai County	Sichuan			

R. pusillus	Ahei Cave	Xishuangbanna	Yunnan			
R. pusillus	Heshang Cave	Kunming, Fumin County	Yunnan	25°12′N	102°28′E	
R. pusillus	Xiangshui Village	Fumin County	Yunnan			
R. pusillus	Wangzhangya Cave	Dawei County	Yunnan			
R. pusillus	Fengjing Cave	Jiuxiang County	Yunnan			
R. pusillus	Jiuxiang Cave	Yiliang County	Yunnan			
R. pusillus	Bailong Cave	Mile County	Yunnan	24°12′N	103°14′E	
R. pusillus	Shaft Cave, near Bailong Cave	Mile County	Yunnan	24°11′N	103°21′E	
R. stheno	Ahei Cave	Xishuang banna	Yunnan			
R. stheno	Jinuo Cave	Xishuang banna	Yunnan	21°58′N	100°49′E	

1 Sun, K.-P. *et al.* A new cryptic species of rhinolophus macrotis (Chiroptera : Rhinolophidae) from Jiangxi Province, China. *Acta Chiropterologica* **10**, 1-10, doi:10.3161/150811008x331045 (2008).

2 Volleth, M. *et al.* Comparative chromosomal studies in Rhinolophus formosae and R-luctus from China and Vietnam: elevation of R-l. lanosus to species rank. *Acta Chiropterologica* **19**, 41-50, doi:10.3161/15081109acc2017.19.1.003 (2017).

3 Jiang, T., Lu, G., Sun, K., Luo, J. & Feng, J. Coexistence of Rhinolophus affinis and Rhinolophus pearsoni revisited. *Acta Theriologica* **58**, 47-53, doi:10.1007/s13364-012-0093-x (2013).

4 Shi, L.-m., Feng, J., Liu, Y., Ye, G.-x. & Zhu, X. Is food resource partitioning responsible for deviation of echolocation call frequencies from allometry in Rhinolophus macrotis? *Acta Theriologica* **54**, 371-382, doi:10.4098/j.at.0001-7051.099.2008 (2009).

5 He, G. Z. *et al.* Entamoeba histolytica Infections in a King Horseshoe Bat (Rhinolophus rex): A First Case Report. *Asian Journal of Animal and Veterinary Advances* **6**, 1026-1030, doi:10.3923/ajava.2011.1026.1030 (2011).

6 Liu, Y., Feng, J., Jiang, Y. L., Wu, L. & Sun, K. P. Vocalization development of greater horseshoe bat, Rhinolophus ferrumequinum (Rhinolophidae, Chiroptera). *Folia Zoologica* **56**, 126-136 (2007).

7 Bush, S. E. & Robbins, R. G. New host and locality records for Ixodes simplex Neumann and Ixodes vespertilionis Koch (Acari: Ixodidae) from bats (Chiroptera: Hipposideridae, Rhinolophidae and Vespertilionidae) in southern China. *International Journal of Acarology* **38**, 1-5, doi:10.1080/01647954.2011.569509 (2012).

8 Flanders, J., Wei, L., Rossiter, S. J. & Zhang, S. Identifying the effects of the Pleistocene on the greater horseshoe bat, Rhinolophus ferrumequinum, in East Asia using ecological niche modelling and phylogenetic analyses. *Journal of Biogeography* **38**, 439-452, doi:10.1111/j.1365-2699.2010.02411.x (2011).

9 Liu, Y., Jiang, T., Berquist, S. & Feng, J. Vocal characters and wing morphology of Rhinolophus marshalli from Tiantang Cave, Guangxi Province, China. *Mammalia* **73**, 373-376, doi:10.1515/mamm.2009.053 (2009).

10 Rossiter, S. J., Benda, P., Dietz, C., Zhang, S. & Jones, G. Rangewide phylogeography in the greater horseshoe bat inferred from microsatellites: implications for population history, taxonomy and conservation. *Molecular Ecology* **16**, 4699-4714, doi:10.1111/j.1365-294X.2007.03546.x (2007).

11 Lei, M., Dong, D., Mu, S., Pan, Y.-H. & Zhang, S. Comparison of Brain Transcriptome of the Greater Horseshoe Bats (Rhinolophus ferrumequinum) in Active and Torpid Episodes. *Plos One* **9**, doi:10.1371/journal.pone.0107746 (2014).

12 Mao, X., He, G., Zhang, J., Rossiter, S. J. & Zhang, S. Lineage Divergence and Historical Gene Flow in the Chinese Horseshoe Bat (Rhinolophus sinicus). *Plos One* **8**, doi:10.1371/journal.pone.0056786 (2013).

13 Jiang, T., Feng, J., Sun, K. & Wang, J. Coexistence of two sympatric and morphologically similar bat species Rhinolophus affinis and Rhinolophus pearsoni. *Progress in Natural Science-Materials International* **18**, 523-532, doi:10.1016/j.pnsc.2007.12.005 (2008).

14 Sun, K. *et al.* The complex evolutionary history of big-eared horseshoe bats (Rhinolophus macrotis complex): insights from genetic, morphological and acoustic data. *Scientific Reports* **6**, doi:10.1038/srep35417 (2016).

15 Ge, X.-Y. *et al.* Coexistence of multiple coronaviruses in several bat colonies in an abandoned mineshaft. *Virologica Sinica* **31**, 31-40, doi:10.1007/s12250-016-3713-9 (2016).

16 Wu, Y. & Vu Dinh, T. A New Species of Rhinolophus (Chiroptera: Rhinolophidae) from China. *Zoological Science* **28**, 235-241, doi:10.2108/zsj.28.235 (2011).

17 Zhang, L. *et al.* Recent surveys of bats (Mammalia: Chiroptera) from China. I. Rhinolophidae and Hipposideridae. *Acta Chiropterologica* **11**, 71-88, doi:10.3161/150811009x465703 (2009).

559 **Table S2.** Mean land cover and land use attributes (and 20% and 80% percentiles) in the
560 surroundings (<30km distance) of bat location and randomly selected points (see methods) within
561 and outside China.

	Bat Locations			***Random in China***			***Random out China***		
	Mean	*20%*	*80%*	*Mean*	*20%*	*80%*	*Mean*	*20%*	*80%*
Livestock Density (heads/km^2)									
- *Chickens*	781	183	931	703	160	841	317	15	317
- *Ducks*	256	18	294	202	10	264	26	0	16
- *Pigs*	99	42	163	107	43	148	18	0	21
- *Goats*	32	0	47	30	4	42	8	0	9
- *Sheep*	5	0	0	3	0	1	14	0	21
- *Cattle*	22	5	31	22	6	32	16	2	21
Forest Cover (%)	45	19	71	35	13	55	52	20	80
Forest Fragmentation ()	73	54	96	83	68	98	61	35	90
Cropland ()	20	5	36	24	6	38	30	3	59
People (cap/km^2)	282	63	318	199	59	270	107	12	114
Villages/Human Settlements ()	11	3	18	10	2	16	4	0	5

562

563

Table S3. Report for the spatially constrained multivariate grouping analysis, showing group numerosity, descriptive statistics and boxplots, in comparison with the global benchmark. The share is calculated as the ratio of the variable range (min-max) which is occupied by the same variable in a group. Q1 and Q3 are respectively the first and third quartile, and sd is the standard deviation. The R2 parameter measures the indicator's performance in grouping the sample, as relative reduction of the intra-group variability w.r.t. the global sample variability. Variables include fragmentation (frg), livestock (lst), and settlements (stl). Boxplots are an intuitive tool to visually recap statistical distributions. The meaning of the elements of boxplots is described in the figure below. In the report, the first and third quartile are expressed respectively as Q1 and Q3. The high number of outliers for livestock and settlements is typical for high-skewness distributions. The boxplots show well how the indicator distributions shift and narrow from the global dataset to single groups. Although in some the standard deviation of one or more indicators is higher than the global benchmark, each group can be considered as homogeneous for at least one parameter.

Boxplot description

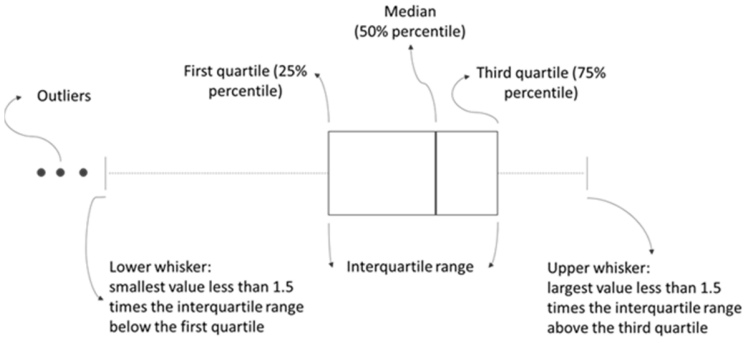

Global

variable	mean	sd	min	max	R2	Q1	median	Q3	
frg	0.69	0.30	0.00	1.00	0.57	0.52	0.78	0.97	
lst	136.53	270.18	-0.25	5520.94	0.56	16.81	59.00	149.64	
stl	0.06	0.09	0.00	0.83	0.49	0.00	0.02	0.07	

Group 1 (Numerosity = 17) - British Isles

variable	mean	sd	min	max	share	Q1	median	Q3	
frg	0.98	0.01	0.94	1.00	0.06	0.98	0.98	1.00	
lst	141.01	81.27	65.69	358.85	0.05	78.74	108.59	196.32	
stl	0.04	0.03	0.01	0.15	0.17	0.02	0.03	0.05	

Group 2 (Numerosity = 6) - East Nepal

variable	mean	sd	min	max	share	Q1	median	Q3	
frg	0.92	0.04	0.87	0.98	0.11	0.90	0.92	0.96	
lst	98.74	64.22	55.71	227.21	0.03	68.17	74.06	89.89	
stl	0.03	0.07	0.00	0.16	0.20	0.00	0.00	0.01	

Group 3 (Numerosity = 2) - Malaysian Borneo

variable	mean	sd	min	max	share	Q1	median	Q3	
frg	0.12	0.00	0.12	0.12	0.00	0.12	0.12	0.12	
lst	3945.26	1180.23	3110.71	4779.81	0.30	3527.99	3945.26	4362.53	
stl	0.00	0.00	0.00	0.00	0.00	0.00	0.00	0.00	

Group 4 (Numerosity = 9) - East Bangladesh									
variable	mean	sd	min	max	share	Q1	median	Q3	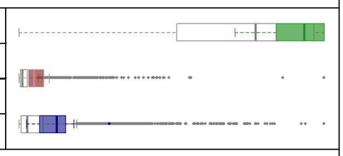
frg	0.91	0.10	0.71	1.00	0.29	0.84	0.94	1.00	
lst	296.63	170.07	74.13	544.77	0.09	166.44	272.83	447.55	
stl	0.10	0.07	0.02	0.25	0.27	0.06	0.10	0.13	
Group 5 (Numerosity = 34) - Southern Sichuan, Guizhou (China)									
variable	mean	sd	min	max	share	Q1	median	Q3	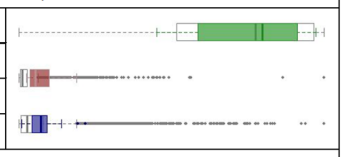
frg	0.75	0.18	0.45	0.97	0.52	0.59	0.80	0.91	
lst	398.06	247.72	134.08	1039.54	0.16	201.37	298.14	539.71	
stl	0.06	0.04	0.01	0.18	0.21	0.04	0.06	0.08	
Group 6 (Numerosity = 188) - Iraq, Iran, Afghanistan									
variable	mean	sd	min	max	share	Q1	median	Q3	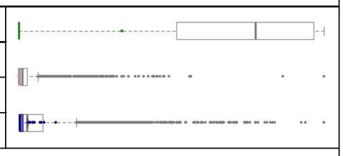
frg	0.00	0.03	0.00	0.34	0.34	0.00	0.00	0.00	
lst	0.05	0.35	0.00	3.08	0.00	0.00	0.00	0.00	
stl	0.01	0.01	0.00	0.10	0.12	0.00	0.00	0.01	
Group 7 (Numerosity = 24) - East China									
variable	mean	sd	min	max	share	Q1	median	Q3	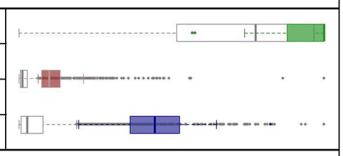
frg	0.92	0.13	0.57	1.00	0.43	0.89	1.00	1.00	
lst	603.50	307.95	0.00	1398.45	0.25	418.57	546.92	736.42	
stl	0.37	0.12	0.16	0.68	0.63	0.31	0.37	0.43	
Group 8 (Numerosity = 185) - Japan, Shanghai to Hong Kong (China)									
variable	mean	sd	min	max	share	Q1	median	Q3	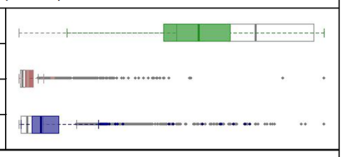
frg	0.57	0.18	0.16	1.00	0.84	0.47	0.59	0.69	
lst	189.25	108.77	16.37	631.17	0.11	110.50	163.29	257.94	
stl	0.10	0.11	0.01	0.63	0.75	0.03	0.06	0.11	
Group 9 (Numerosity = 4) - Manila bay (Philippines)									
variable	mean	sd	min	max	share	Q1	median	Q3	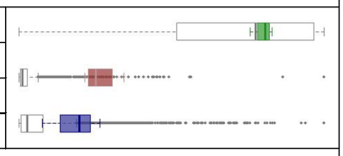
frg	0.80	0.03	0.76	0.83	0.07	0.79	0.81	0.81	
lst	1469.36	307.68	1193.82	1899.49	0.13	1286.61	1392.07	1574.83	
stl	0.15	0.07	0.06	0.22	0.19	0.14	0.16	0.18	
Group 10 (Numerosity = 13) - Central Sichuan (China)									
variable	mean	sd	min	max	share	Q1	median	Q3	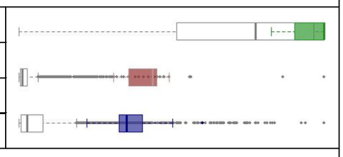
frg	0.96	0.06	0.83	1.00	0.17	0.90	1.00	1.00	
lst	2259.48	335.99	1713.00	2720.77	0.18	1986.94	2412.74	2489.97	
stl	0.32	0.08	0.18	0.50	0.38	0.27	0.29	0.34	
Group 11 (Numerosity = 118) - Northern Myanmar									
variable	mean	sd	min	max	share	Q1	median	Q3	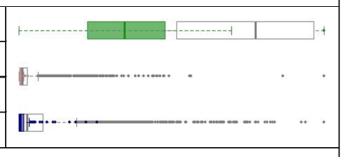
frg	0.35	0.18	0.00	1.00	1.00	0.23	0.35	0.48	
lst	26.58	23.05	0.13	152.78	0.03	9.94	19.75	38.37	
stl	0.02	0.03	0.00	0.21	0.26	0.00	0.00	0.01	
Group 12 (Numerosity = 18) - Lebanon, Syria									
variable	mean	sd	min	max	share	Q1	median	Q3	
frg	0.80	0.38	0.00	1.00	1.00	0.88	1.00	1.00	
lst	50.82	76.73	0.00	204.68	0.04	0.00	2.57	88.93	
stl	0.06	0.04	0.01	0.16	0.19	0.03	0.06	0.08	

579

Group 13 (Numerosity = 41) - East Sichuan (China)									
variable	mean	sd	min	max	share	Q1	median	Q3	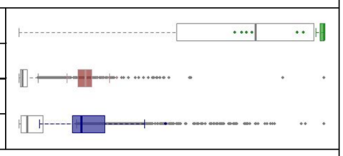
frg	0.97	0.08	0.71	1.00	0.29	0.99	1.00	1.00	
lst	1207.95	196.18	865.09	1768.76	0.16	1063.81	1195.58	1315.51	
stl	0.19	0.07	0.06	0.40	0.41	0.14	0.17	0.23	
Group 14 (Numerosity = 732) - China									
variable	mean	sd	min	max	share	Q1	median	Q3	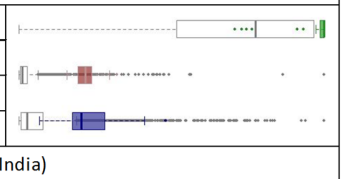
frg	0.85	0.14	0.29	1.00	0.71	0.77	0.89	0.97	
lst	260.33	188.99	63.54	1636.25	0.28	144.39	193.75	300.04	
stl	0.11	0.09	0.00	0.64	0.77	0.04	0.08	0.14	
Group 15 (Numerosity = 14) - West Assam, Sikkim, Bihar (India)									
variable	mean	sd	min	max	share	Q1	median	Q3	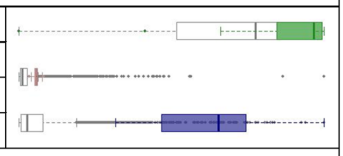
frg	0.83	0.29	0.00	1.00	1.00	0.86	0.97	0.99	
lst	306.08	69.22	186.08	442.16	0.05	279.78	298.44	335.38	
stl	0.52	0.16	0.26	0.83	0.68	0.40	0.54	0.61	
Group 16 (Numerosity = 27) - Atlas Mountains									
variable	mean	sd	min	max	share	Q1	median	Q3	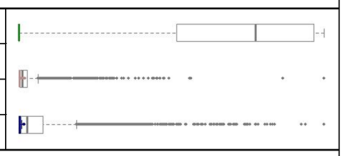
frg	0.00	0.00	0.00	0.00	0.00	0.00	0.00	0.00	
lst	20.45	26.97	3.17	103.64	0.02	4.84	8.10	19.57	
stl	0.00	0.00	0.00	0.01	0.02	0.00	0.00	0.00	
Group 17 (Numerosity = 14) - Assam (India)									
variable	mean	sd	min	max	share	Q1	median	Q3	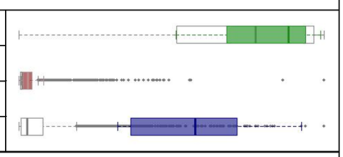
frg	0.82	0.16	0.52	0.99	0.47	0.70	0.88	0.94	
lst	176.63	115.38	36.71	440.25	0.07	82.13	156.77	228.82	
stl	0.47	0.16	0.27	0.77	0.60	0.31	0.48	0.59	
Group 18 (Numerosity = 69) - Australia, South Papua									
variable	mean	sd	min	max	share	Q1	median	Q3	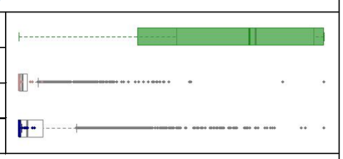
frg	0.69	0.29	0.00	1.00	1.00	0.39	0.76	1.00	
lst	18.32	62.87	0.00	419.57	0.08	0.00	0.65	9.82	
stl	0.00	0.01	0.00	0.04	0.05	0.00	0.00	0.00	
Group 19 (Numerosity = 84) - Philippines, Taiwan									
variable	mean	sd	min	max	share	Q1	median	Q3	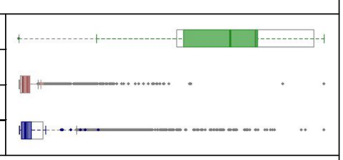
frg	0.63	0.23	0.00	1.00	1.00	0.54	0.69	0.78	
lst	135.73	107.16	10.45	427.88	0.08	51.91	103.28	189.72	
stl	0.03	0.05	0.00	0.22	0.26	0.01	0.02	0.03	
Group 20 (Numerosity = 294) - Borneo, Sulawesi, Papua									
variable	mean	sd	min	max	share	Q1	median	Q3	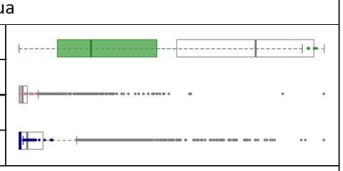
frg	0.32	0.24	0.00	0.98	0.98	0.13	0.24	0.45	
lst	20.76	66.09	0.00	877.45	0.16	1.85	4.46	11.72	
stl	0.01	0.01	0.00	0.09	0.11	0.00	0.00	0.00	
Group 21 (Numerosity = 39) India									
variable	mean	sd	min	max	share	Q1	median	Q3	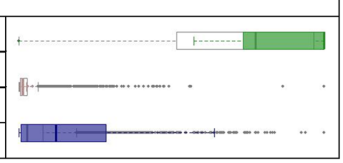
frg	0.85	0.25	0.00	1.00	1.00	0.73	1.00	1.00	
lst	69.90	42.61	12.35	239.52	0.04	41.12	66.94	85.47	
stl	0.13	0.14	0.00	0.53	0.64	0.00	0.10	0.24	

580

Group 22 (Numerosity = 320) - Italy, Central Europe, Balkans									
variable	mean	sd	min	max	share	Q1	median	Q3	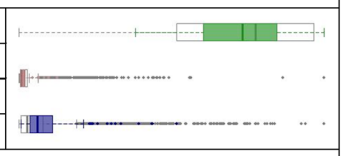
frg	0.73	0.16	0.38	1.00	0.62	0.60	0.73	0.84	
lst	81.91	74.65	4.53	695.83	0.13	37.22	73.12	105.16	
stl	0.07	0.06	0.00	0.43	0.51	0.03	0.05	0.09	
Group 23 (Numerosity = 26) - Saudi Arabia									
variable	mean	sd	min	max	share	Q1	median	Q3	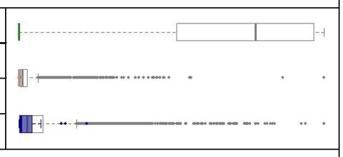
frg	0.00	0.00	0.00	0.00	0.00	0.00	0.00	0.00	
lst	2.09	8.76	-0.25	43.76	0.01	0.00	0.00	0.00	
stl	0.03	0.05	0.00	0.18	0.22	0.00	0.01	0.03	
Group 24 (Numerosity = 1) - Shijiazhuang (Hebei, China)									
variable	mean	sd	min	max	share	Q1	median	Q3	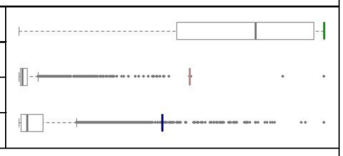
frg	1.00	NA	1.00	1.00	0.00	1.00	1.00	1.00	
lst	3084.02	NA	3084.02	3084.02	0.00	3084.02	3084.02	3084.02	
stl	0.39	NA	0.39	0.39	0.00	0.39	0.39	0.39	
Group 25 (Numerosity = 1202) - Southeast Asia, Sumatra, Java									
variable	mean	sd	min	max	share	Q1	median	Q3	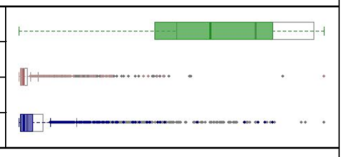
frg	0.63	0.24	0.00	1.00	1.00	0.45	0.63	0.83	
lst	118.12	287.24	0.00	5520.94	1.00	21.93	45.12	95.65	
stl	0.03	0.07	0.00	0.69	0.83	0.00	0.01	0.04	
Group 26 (Numerosity = 283) - Easy Myanmar, South Yunnan (China)									
variable	mean	sd	min	max	share	Q1	median	Q3	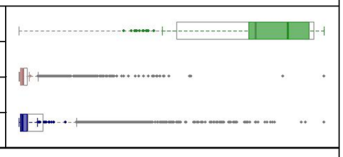
frg	0.83	0.16	0.34	1.00	0.66	0.75	0.88	0.95	
lst	60.25	46.74	3.56	211.33	0.04	22.65	50.62	85.02	
stl	0.02	0.02	0.00	0.13	0.15	0.00	0.01	0.02	
Group 27 (Numerosity = 18) - Henan, Shandong (China)									
variable	mean	sd	min	max	share	Q1	median	Q3	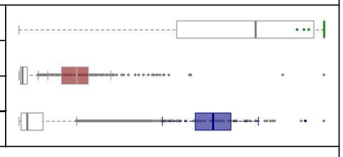
frg	0.99	0.03	0.91	1.00	0.09	1.00	1.00	1.00	
lst	1030.48	298.09	519.25	1664.13	0.21	782.27	1045.74	1210.37	
stl	0.54	0.10	0.39	0.78	0.47	0.48	0.53	0.57	
Group 28 (Numerosity = 716) - Eastern Europe, Asia, West Myanmar									
variable	mean	sd	min	max	share	Q1	median	Q3	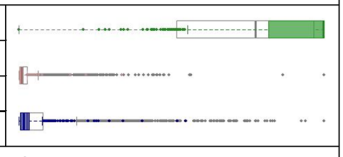
frg	0.87	0.23	0.00	1.00	1.00	0.82	1.00	1.00	
lst	49.40	105.81	0.00	1861.40	0.34	3.04	22.39	60.20	
stl	0.02	0.04	0.00	0.45	0.55	0.00	0.01	0.03	
Group 29 (Numerosity = 153) - Yunnan, Central to Northeast China									
variable	mean	sd	min	max	share	Q1	median	Q3	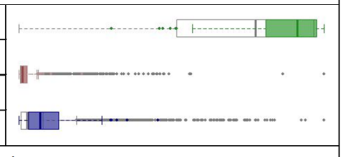
frg	0.87	0.14	0.30	1.00	0.70	0.81	0.91	0.98	
lst	122.43	135.54	1.24	1137.94	0.21	35.82	104.68	147.99	
stl	0.08	0.07	0.00	0.38	0.46	0.03	0.06	0.11	
Group 30 (Numerosity = 349) - Western Europe, Maghreb									
variable	mean	sd	min	max	share	Q1	median	Q3	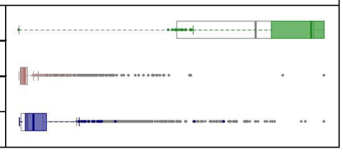
frg	0.88	0.16	0.00	1.00	1.00	0.83	0.96	1.00	
lst	105.59	132.63	2.48	1040.61	0.19	34.59	64.49	125.01	
stl	0.06	0.06	0.00	0.56	0.67	0.02	0.04	0.07	

581

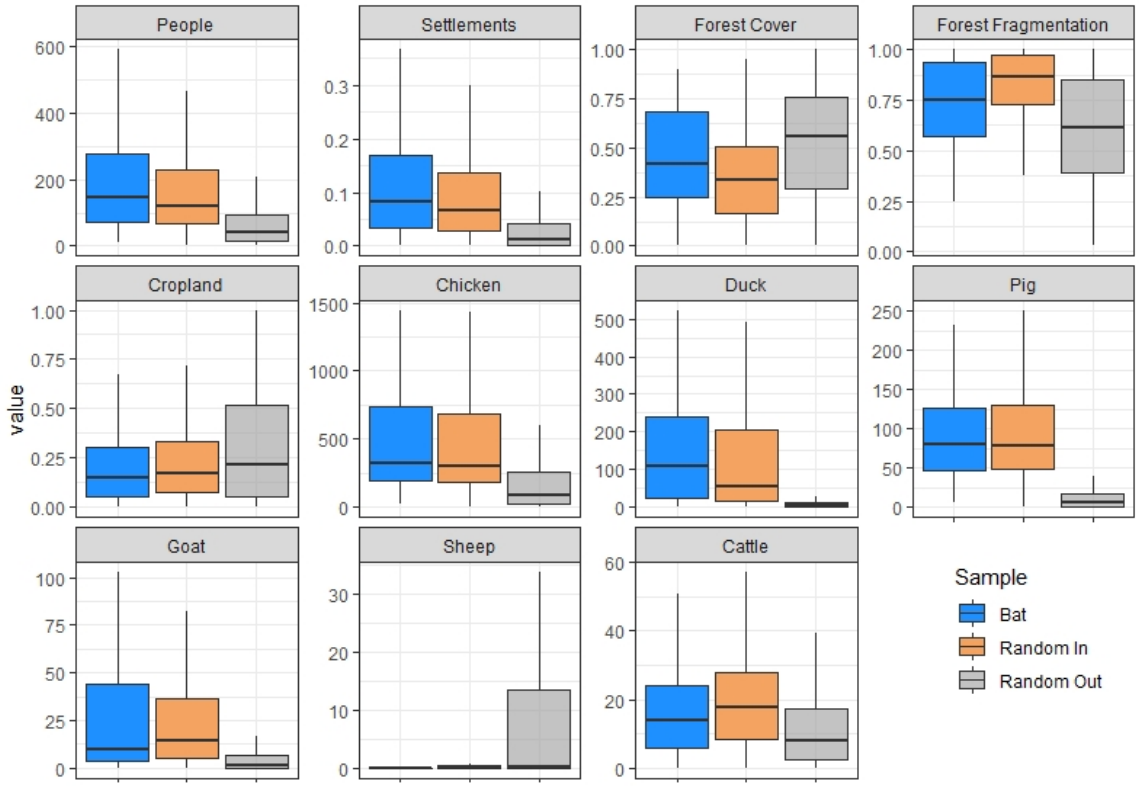

Figure S1. Boxplots of the distribution data of indicators. In blue are reported data in bat locations, in orange data in China, in grey data outside China.

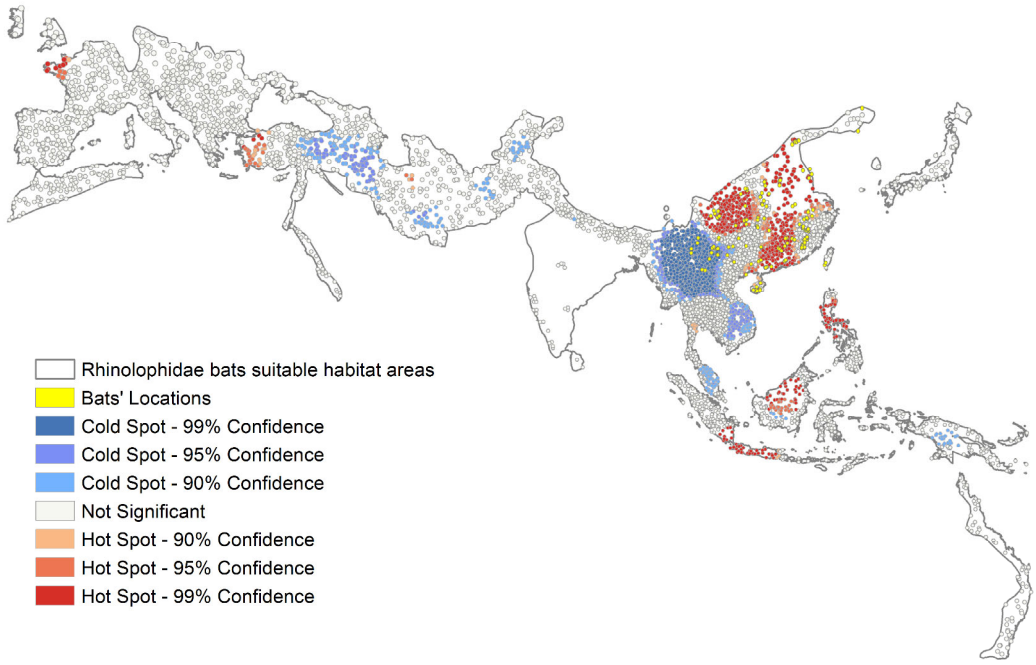

Figure S2. Hotspots and coldspots of chicken density.

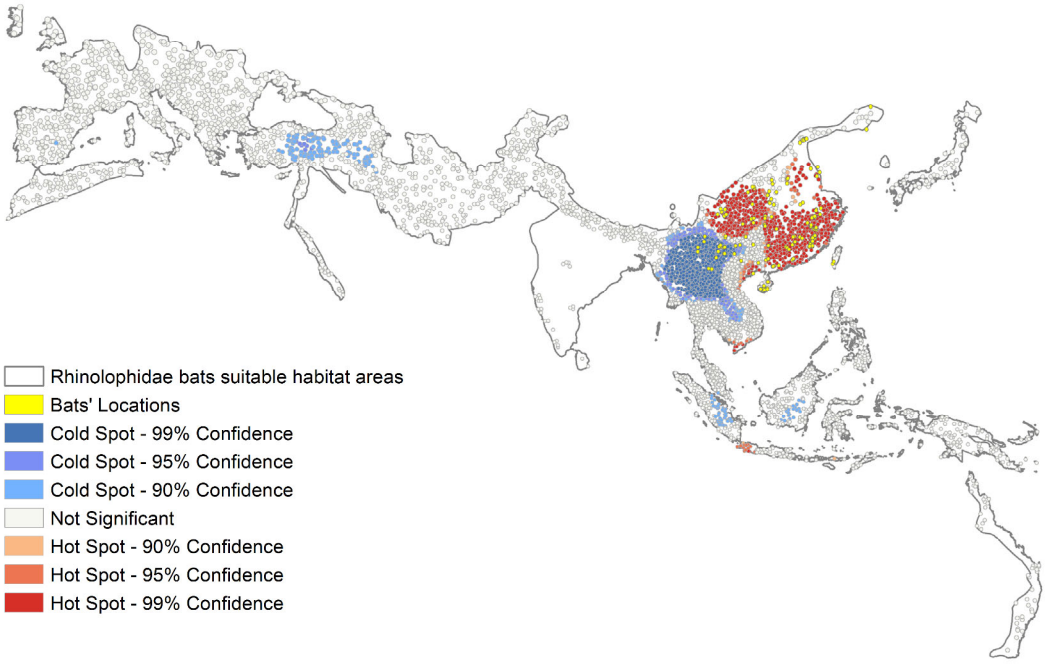

Figure S3. Hotspots and coldspots of duck density.

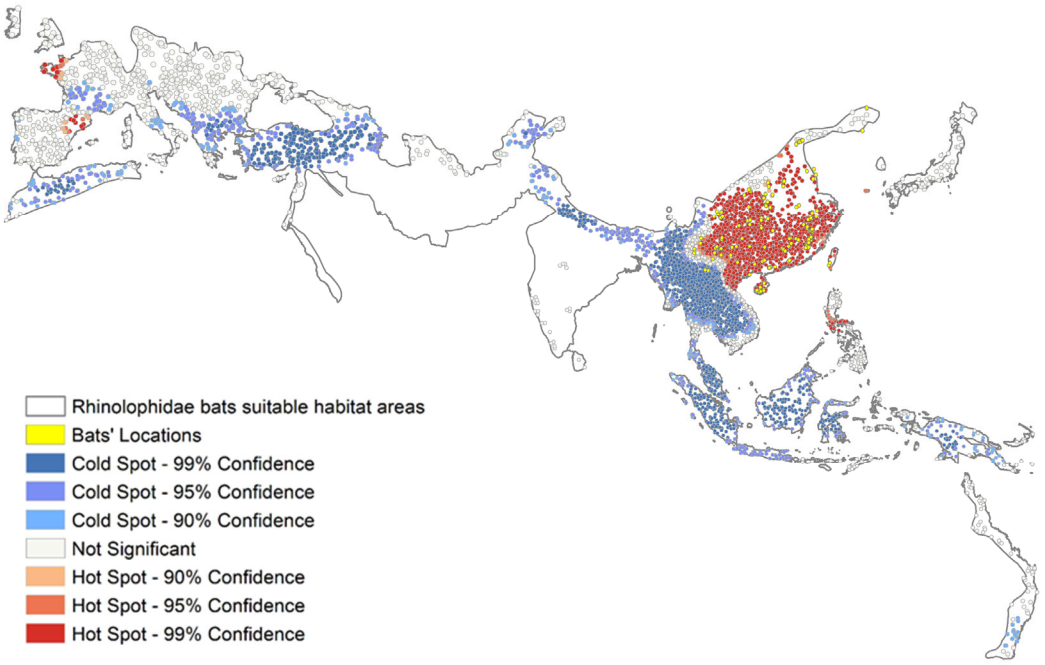

591
592 **Figure S4.** Hotspots and coldspots of pig density.

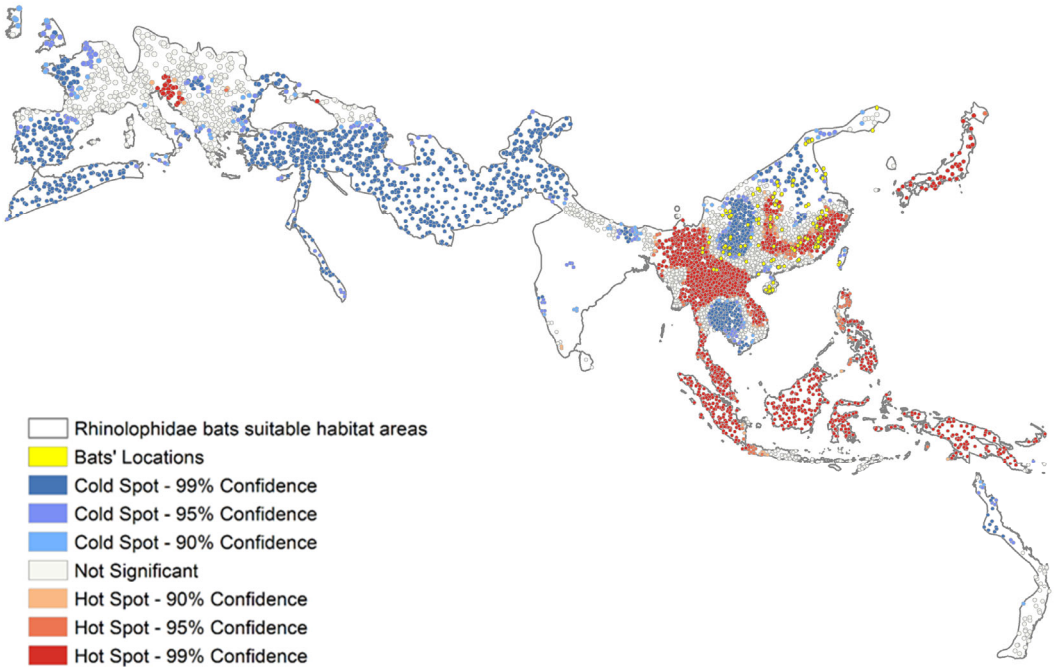

593

594 **Figure S5.** Hotspots and coldspots of forest cover

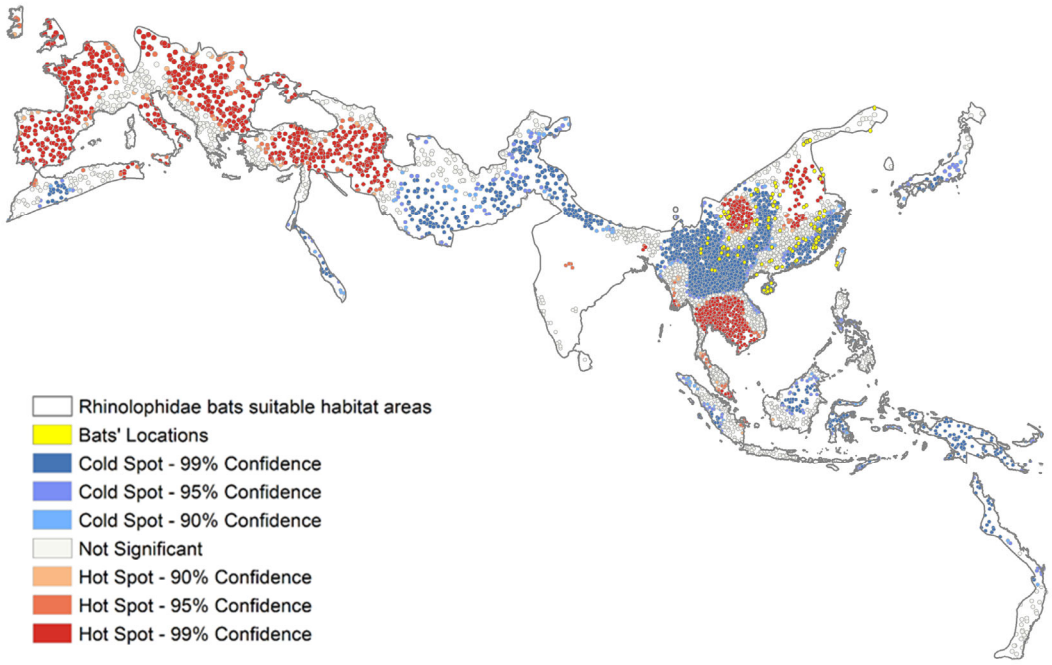

595

596 **Figure S6.** Hotspots and coldspots of cropland cover.

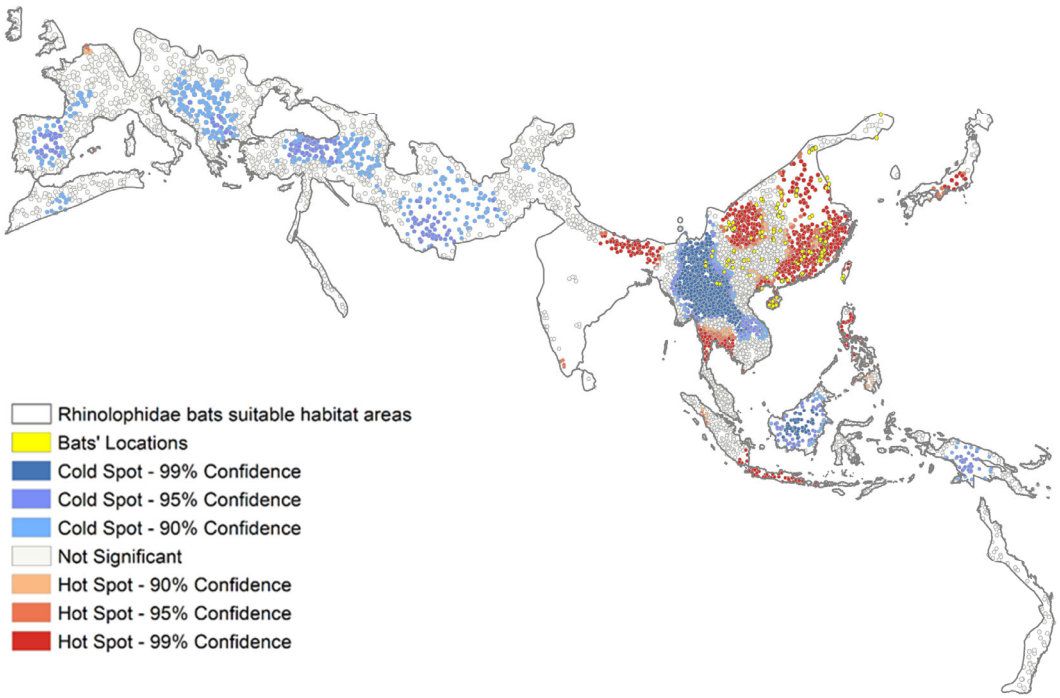

597
598 **Figure S7.** Hotspots and coldspots of population density.

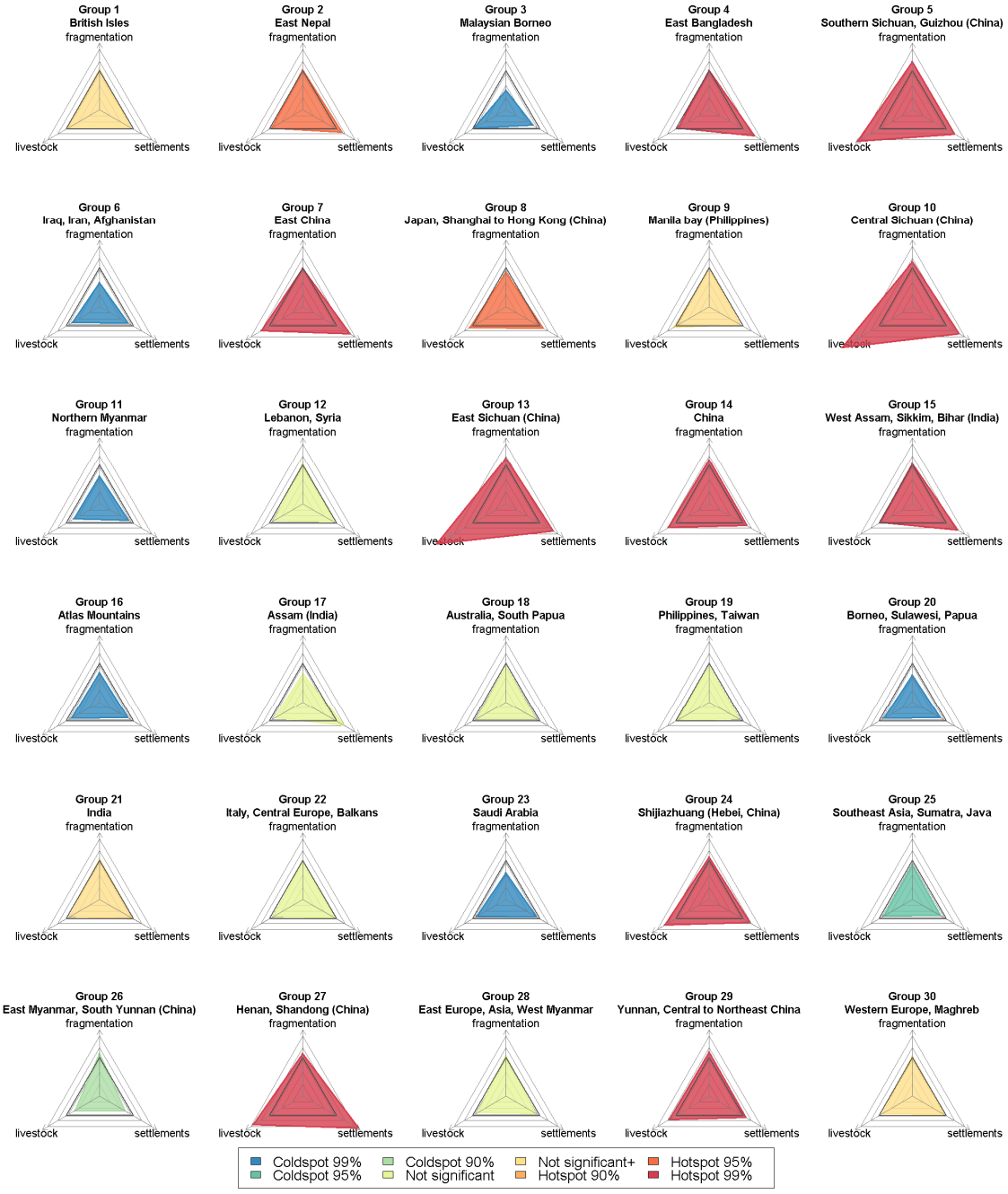

Figure S8. Group analysis. Trajectories of risk.